nature neuroscience

ARTICLES

Microglia emerge from erythromyeloid precursors via Pu.1- and Irf8-dependent pathways

Katrin Kierdorf[1,2], Daniel Erny[1], Tobias Goldmann[1], Victor Sander[1], Christian Schulz[3,4], Elisa Gomez Perdiguero[3,4], Peter Wieghofer[1,2], Annette Heinrich[5], Pia Riemke[6], Christoph Hölscher[7,8], Dominik N Müller[9], Bruno Luckow[10], Thomas Brocker[11], Katharina Debowski[12], Günter Fritz[1], Ghislain Opdenakker[13], Andreas Diefenbach[14], Knut Biber[5,15], Mathias Heikenwalder[16], Frederic Geissmann[3,4], Frank Rosenbauer[6] & Marco Prinz[1,17]

Microglia are crucial for immune responses in the brain. Although their origin from the yolk sac has been recognized for some time, their precise precursors and the transcription program that is used are not known. We found that mouse microglia were derived from primitive c-kit$^+$ erythromyeloid precursors that were detected in the yolk sac as early as 8 d post conception. These precursors developed into CD45$^+$ c-kit^{lo} CX$_3$CR1$^-$ immature (A1) cells and matured into CD45$^+$ c-kit$^-$ CX$_3$CR1$^+$ (A2) cells, as evidenced by the downregulation of CD31 and concomitant upregulation of F4/80 and macrophage colony stimulating factor receptor (MCSF-R). Proliferating A2 cells became microglia and invaded the developing brain using specific matrix metalloproteinases. Notably, microgliogenesis was not only dependent on the transcription factor Pu.1 (also known as Sfpi), but also required Irf8, which was vital for the development of the A2 population, whereas Myb, Id2, Batf3 and Klf4 were not required. Our data provide cellular and molecular insights into the origin and development of microglia.

Microglia are the tissue macrophages of the brain and scavenge dying cells, pathogens and molecules using pattern recognition receptors and subsequent phagocytosis and endocytosis[1–3]. Unlike macroglia (astrocytes and oligodendrocytes) and neurons, which are derived from the neuroectoderm, microglia progenitors arise from the peripheral mesodermal tissue[4,5]. Their origin from the yolk sac, which was proposed in 1999 (ref. 6), was confirmed by two recent fate-mapping studies[7,8]. One study used a tamoxifen-inducible Cre recombinase under the control of Runx1, a transcription factor involved in the development of all lineages of normal hematopoiesis[7]. In a more recent study, we found that microglia were derived from MCSF-R–expressing yolk sac precursors that were present between 8.5 and 9.5 days post conception (dpc)[8]. However, these studies focused on already committed CX$_3$CR1-expressing yolk sac myeloid cells and therefore considered immature macrophages to be microglia precursors, thereby missing possible earlier progenitors that lack macrophage markers such as F4/80 and CD11b.

We found that uncommitted c-kit$^+$ stem cells that have both erythroid and myeloid potential are the direct yolk sac–derived precursors of microglia during early embryogenesis. These primitive cells have the ability to give rise to microglia and macrophages *in vitro* and *in vivo* under defined conditions. During their journey into the developing CNS, these cells acquired macrophage-specific markers and finally settled in the target tissue, where they differentiated into definitive microglia with fine processes. Of note, this extremely complex developmental process required specific molecules that could be identified at defined time points. Our results describe microglia as a distinct tissue-specific macrophage population that is clearly genetically different from circulating myeloid cells.

RESULTS

c-kit$^+$ erythromyeloid cells are the microglia progenitors

To follow the fate of late myeloid cells in the brain during embryogenesis, we used *Cx3cr1*$^{GFP/wt}$ mice, which have a GFP knock-in on one allele of the *Cx3cr1* gene. CX$_3$CR1 is expressed in mature monocytes and in a subset of peripheral mononuclear phagocytes. In the brain, only microglia express this marker[9,10].

We first addressed the question of the origin of *Cx3cr1*$^{GFP/wt}$ microglia progenitors in the mouse embryo. It has been shown that hematopoietic cells can be independently generated in two distinct sites.

[1]Department of Neuropathology, University of Freiburg, Freiburg, Germany. [2]Faculty of Biology, University of Freiburg, Freiburg, Germany. [3]Centre for Molecular and Cellular Biology of Inflammation, King's College London, London, UK. [4]Peter Gorer Department of Immunobiology, King's College London, London, UK. [5]Department of Psychiatry, University of Freiburg, Freiburg, Germany. [6]Institute of Molecular Tumor Biology, University of Muenster, Muenster, Germany. [7]Division of Infection Immunology, Research Center Borstel, Borstel, Germany. [8]Cluster of Excellence, Inflammation at Interfaces (Borstel-Kiel-Lübeck-Plön), Kiel, Germany. [9]Experimental and Clinical Research Center, Charité Medical Faculty and the Max-Delbrück Center for Molecular Medicine, Berlin, Germany. [10]Klinikum der Universität München, Medizinische Klinik und Poliklinik IV, Arbeitsgruppe Klinische Biochemie, München, Germany. [11]Institute for Immunology, Ludwig-Maximilians-Universität München, Munich, Germany. [12]Cell Research Group, German Primate Center, Göttingen, Germany. [13]Department of Microbiology and Immunology, Rega Institute for Medical Research, University of Leuven, Belgium. [14]Department of Microbiology, University of Freiburg, Freiburg, Germany. [15]Department of Neuroscience, University Medical Center Groningen, Groningen, The Netherlands. [16]Institute of Virology, Technische Universität München/Helmholtz-Zentrum Munich, Munich, Germany. [17]Center for Biological Signaling Studies, University of Freiburg, Freiburg, Germany. Correspondence should be addressed to M.P. (marco.prinz@uniklinik-freiburg.de).

Received 6 November 2012; accepted 21 December 2012; published online 20 January 2013; corrected online 6 February 2013 (details online); doi:10.1038/nn.3318

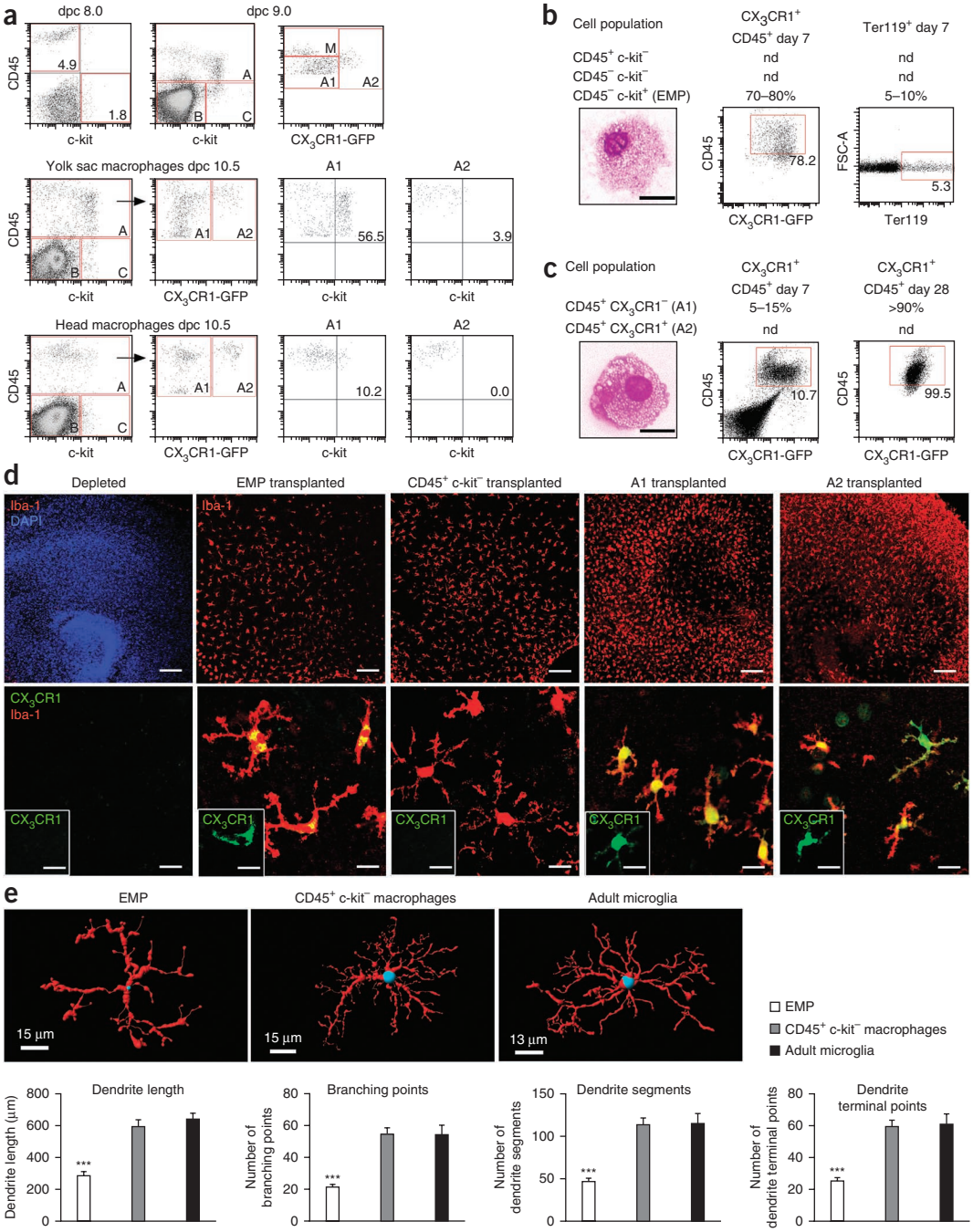

Figure 1 Identification and characterization of the microglia progenitor. (**a**) Top, fractionation of 8.0-dpc yolk sac cells using CD45 and c-kit markers allowed for distinction of separate subsets of precursor cells by fluorescence-activated cell sorting (FACS, left). We analyzed 9.0-dpc yolk sac from a male *Cx3cr1*$^{GFP/GFP}$ and female *Cx3cr1*$^{wt/wt}$ mating (right). Separation of CD45$^+$ cells allowed for discrimination of two subsets designated A1 (CX_3CR1-GFP$^-$) and A2 (CX_3CR1-GFP$^+$) and a maternal (M) CD45$^+$ CX_3CR1-GFP$^-$ population. Middle and bottom, characterization of myeloid precursors in the yolk sac and the head at 10.5 dpc. In the CD45-expressing cells in the brain, GFP$^+$ and GFP$^-$ populations were found. The CD45 fraction in the yolk sac can be further subdivided according to different levels of c-kit expression, namely into CD45$^+$ c-kit$^-$ and CD45$^+$ c-kit$^+$ in A1 and a single CD45$^+$ c-kit$^-$ population in A2. Data are representative of four independent experiments. Percentages are indicated. (**b**) *In vitro* differentiation potential of 8.0-dpc yolk sac subsets defined in **a**. The hematopoietic potential was strictly ascribed to the CD45$^-$ c-kit$^+$ subset that comprised myeloid and erythroid precursors, a characteristic feature of EMPs. Data are representative of three independent experiments. nd, not detectable. (**c**) *In vitro* differentiation potential of 9.0-dpc yolk sac populations shown in **a**. Only c-kit$^+$ A1 cells differentiated into the myeloid lineage at the indicated time points. Representative dot plots are depicted. Morphology of the cultured cells is illustrated with Pappenheim staining. Data are representative of two independent experiments. (**d**) Differentiation of adoptively transferred yolk sac subsets on organotypic hippocampal brain slice cultures depleted of endogenous microglia before cell transfer. At 12 d in culture, transferred yolk sac cells from embryos of a male *Cx3cr1*$^{GFP/GFP}$ and female *Cx3cr1*$^{wt/wt}$ cross-breeding were analyzed using the macrophage marker Iba-1 and CX_3CR1-GFP. Scale bars represent 200 µm (top panels) and 20 µm (bottom panels and insets). Data are representative of three independent experiments. (**e**) Three-dimensional reconstruction (top) and Imaris-based automatic quantification of cell morphology (bottom) of transferred cells. Data represent means ± s.e.m. of at least five cells per group. ***$P < 0.001$. Data are representative of two independent experiments.

The first site, the yolk sac, generates erythroid cells and macrophages starting at 7.5–8.0 dpc, that is, before microglia progenitors are first detected in the neural folds[11–13]. To determine whether the yolk sac contains progenitor cells with macrophage properties, we analyzed the yolk sac by flow cytometry. Consistent with an earlier report[14], three subsets of cells could be discriminated in the 8.0-dpc yolk sac, namely the CD45$^+$ c-kit$^-$, CD45$^-$ c-kit$^+$ and CD45$^-$ c-kit$^-$ populations (**Fig. 1a**). At this time point, none of the three cell populations expressed the CX_3CR1-GFP reporter (data not shown). Notably, analysis of the 9.0-dpc yolk sac allowed us to distinguish between CD45$^+$ c-kit$^-$ cells, CD45$^-$ c-kit$^-$ and CD45$^-$ c-kit$^+$ cells. By separation of CD45$^+$ cells, we were able to discriminate between two subsets, designated A1 (CX_3CR1-GFP$^-$) and A2 (CX_3CR1-GFP$^+$), as well as a maternal CD45$^+$ CX_3CR1-GFP$^-$ population. Notably, 10.5-dpc macrophages in the head had further matured in comparison to the yolk sac as evidenced by the downregulation of c-kit in A1 and A2 cells.

To examine the differentiation potential of yolk sac cells found at 8.0 and 9.0 dpc, we sorted cells on the basis of CD45 and c-kit expression (**Fig. 1b**) or CD45 and CX_3CR1 expression, respectively (**Fig. 1c**). In the early yolk sac (8.0 dpc), only CD45$^-$ c-kit$^+$ cells, but not CD45$^+$ c-kit$^-$ or CD45$^-$ c-kit$^-$ cells, were able to give rise to both CX_3CR1^+ CD45$^+$ macrophages and Ter119$^+$ erythrocytes *in vitro,* which is characteristic of erythromyeloid progenitors (EMPs; **Fig. 1b**), confirming earlier observations[14]. In contrast, later yolk sac populations (9.0 dpc) showed only poor (A1) or no (A2) macrophage differentiation potential after 7 d of differentiation *in vitro* (**Fig. 1c**). We therefore considered the CD45$^-$ c-kit$^+$ EMPs to be the earliest potential yolk sac progenitors that could act as the direct microglia precursors. To test the potential of yolk sac cells to differentiate into microglia cells *in situ*, we used microglia-free organotypic hippocampal slice cultures (OHSCs) as described previously[15] (**Fig. 1d**). Sorted yolk sac cell populations were adoptively transferred onto OHSCs and the expression of Iba-1 and CX_3CR1-GFP was assessed after 12 d. Only A1 and A2 cells from the late yolk sac and EMPs from the early yolk sac differentiated into Iba-1$^+$ CX_3CR1-GFP$^+$ cells with typical microglia morphology. In contrast, early maternal CD45$^+$ c-kit$^-$ cells did not generate arborized Iba-1$^+$ cells expressing CX_3CR1-GFP. Notably, unbiased quantitative morphometric three-dimensional measurements revealed that transferred EMPs differentiated into Iba-1$^+$ CX_3CR1^+ cells with shorter processes, underscoring the premature nature of early EMPs (**Fig. 1e**).

Microglia develop independently from maternal macrophages

To determine whether maternal CD45$^+$ c-kit$^-$ cells may contribute to the microglia pool in the embryo, we examined the fate of maternally derived cells in *Cx3cr1*$^{wt/wt}$ embryos resulting from the cross breeding of *Cx3cr1*$^{GFP/wt}$ female and *Cx3cr1*$^{wt/wt}$ male mice (**Fig. 2a**,**b**). As expected, only the maternally derived CD45$^+$ cells expressed GFP at 9.0 dpc. Notably, we did not detect any GFP$^+$ cells in the brain, meninges and choroid plexus (**Supplementary Fig. 1**) of the resulting

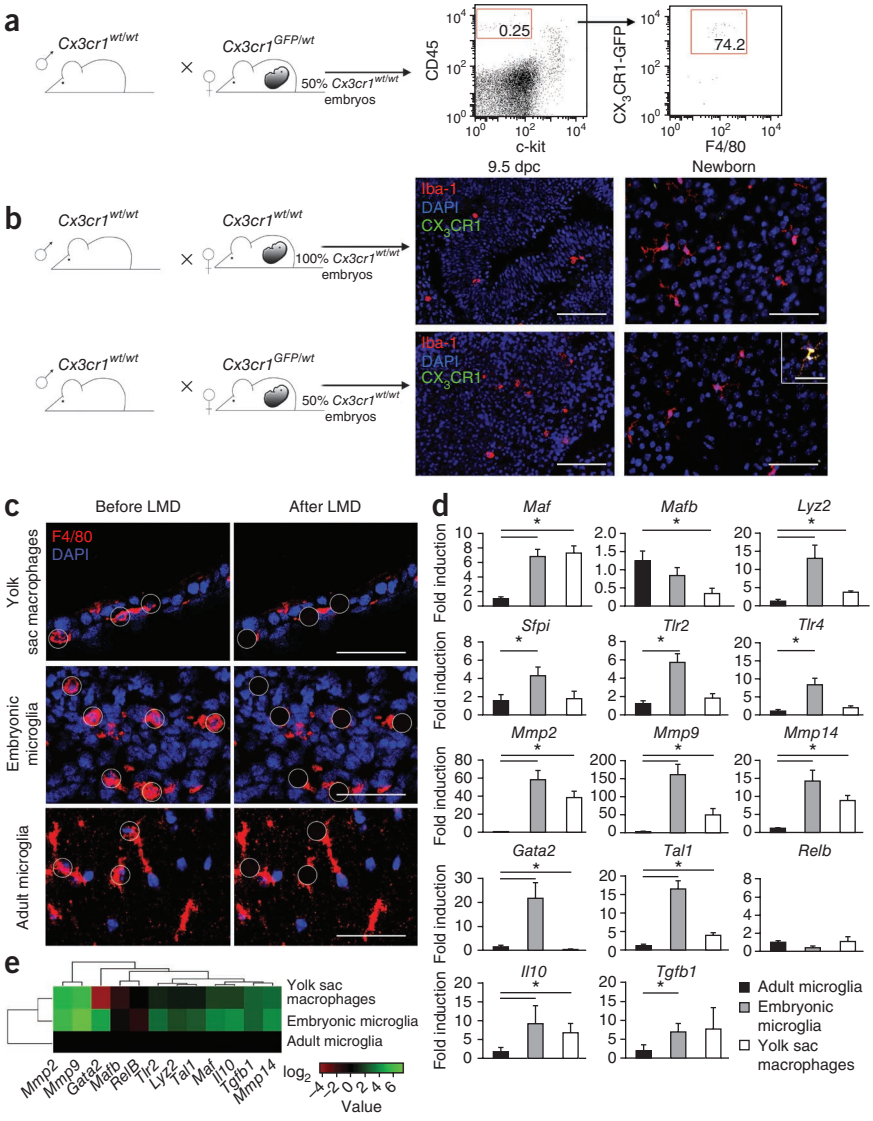

Figure 2 Characterization of maternal and yolk sac macrophages during development. (**a**) At 9.0 dpc, a population of maternally derived CD45$^+$ c-kit$^-$ cells expressed the myeloid differentiation marker F4/80. In *Cx3cr1*$^{wt/wt}$ embryos, resulting from a *Cx3cr1*$^{GFP/wt}$ (female) and *Cx3cr1*$^{wt/wt}$ (male) cross-breeding, only the maternally derived CD45$^+$ cells were GFP$^+$. (**b**) Direct fluorescent microscopic visualization revealed no maternal GFP$^+$ cells in the 9.5-dpc embryonic neuroectoderm (left) or in the newborn brain (right). Iba-1 immunoreactivity (red) for microglia/macrophages and DAPI staining for nuclei (blue). Scale bars represent 100 µm. Inset, Iba-1$^+$ CX_3CR1-GFP$^+$ parenchymal microglia from a *Cx3cr1*$^{GFP/wt}$ littermate. Scale bar represents 20 µm. (**c**) Laser microdissection (LMD) of F4/80$^+$ (red) yolk sac macrophages at 14.0 dpc, embryonic microglia at 14.0 dpc and adult microglia (P60). DAPI was used to stain nuclei (blue). The locations of cells before (left) and after (right) microdissection are shown. Scale bars represent 50 µm. (**d**) Quantification of transcripts in microdissected F4/80$^+$ cells. Data represent means ± s.e.m. with four to six mice in each group. $^*P < 0.05$. (**e**) Quantitative RT-PCR data are presented on a $\log_2$ scale (red/brown, downregulated; green, upregulated). Rows indicate the expression value of grouped mice and columns represent particular genes. Each data point reflects the median expression value of a particular gene resulting from four to six mice, normalized to the mean expression value of the respective gene in adult microglia.

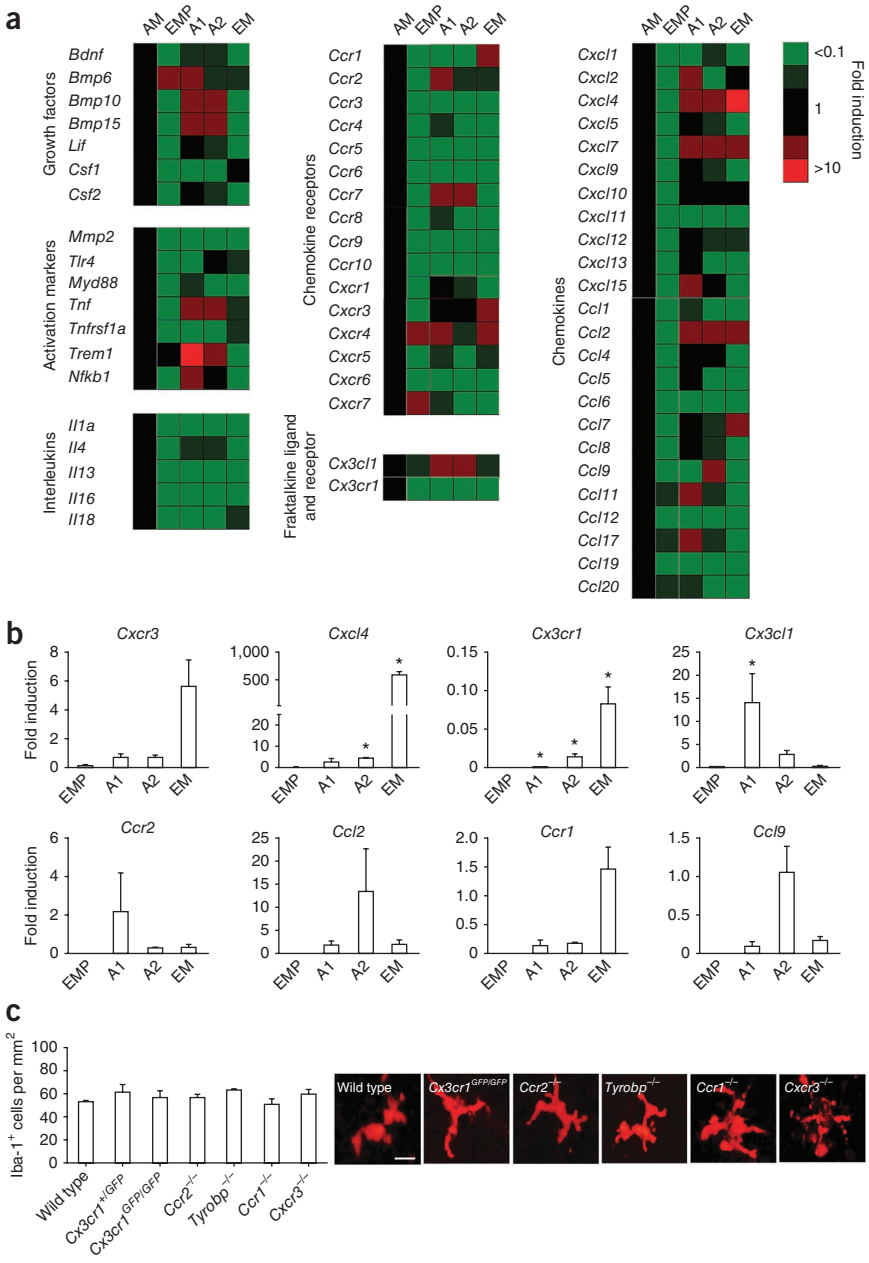

Figure 3 Regulation and function of chemokine receptors during microgliogenesis. (**a**) Heat maps of transcripts in FACS-sorted adult microglia (AM), EMPs, A1 and A2 myeloid precursors, and embryonic microglia (EM) (14.0 dpc). Data are expressed as fold induction (brown/red) or reduction (green). Each data point reflects the median expression value of a particular gene resulting from three mice normalized to the mean expression value of the gene in adult microglia. (**b**) Quantitative RT-PCR of indicated genes on isolated cells. Bars represent means ± s.e.m. with three mice in each group. $*P < 0.05$. (**c**) Normal development and morphology of microglia in the absence of CCR1, CCR2, CX_3CR1, CXCR3 or Tyrobp at 14.0 dpc. Left, semi-quantitative examination of Iba-1$^+$ parenchymal microglia. Data are expressed as means ± s.e.m. Three sections of at least four mice were examined for each group. Right, Iba-1 immunohistochemistry (red) revealed no morphological abnormalities in the absence of the designated genes. Scale bar represents 20 μm.

Cx3cr1$^{wt/wt}$ embryo, excluding a contribution of maternally derived cells to the microglia pool in the progeny. We did not further examine the fate of maternal macrophages in the embryo that might be involved in the immune response of the embryo outside the brain. In sum, these experiments allowed us to identify three independent cell populations in the early yolk sac, namely maternal CD45$^+$ c-kit$^-$ and CD45$^-$ c-kit$^-$ cells, neither of which contributed to the microglia pool of the embryo, and CD45$^-$ c-kit$^+$ EMPs, which constituted the genuine microglia precursors in the yolk sac.

Having identified the specific microglia precursors in the developing yolk sac, we further examined microglia development in the neuroectoderm. To do so, we performed direct microscopic immunofluorescence visualization in the developing neural tube using a panel of surface markers (**Supplementary Fig. 2**). Although embryos at 8.0 dpc did not display CX_3CR1-GFP$^+$ cells in the neural folds or adjacent mesenchyme, most embryos from 9.0 dpc contained round CX_3CR1-GFP$^+$ cells in the mesenchyme surrounding the nestin$^+$ neural tube (**Supplementary Fig. 2a**). Starting at 9.5 dpc, ameboid CX_3CR1-GFP$^+$ cells began to colonize the neural tube, and showed typical microglia morphology as early as 14.0 dpc. At 9.0 dpc, microglia progenitors clearly expressed CD45 (**Supplementary Fig. 2b**) and the macrophage marker F4/80 (**Supplementary Fig. 2c**). Notably, following entry into the neural tube, ameboid microglia began losing F4/80 expression and showed signs of phagocytosis, with frequent uptake of DAPI-positive dying cells (most likely neurons) accompanied by strong lysosomal-associated membrane protein 2 signals (**Supplementary Fig. 2d**). The macrophage marker Iba-1 was highly expressed on all seeded amoeboid microglia and on CX_3CR1-GFP$^+$ macrophages in the mesenchyme at 9.5 dpc (**Supplementary Fig. 2e**), partially near developing vessels (**Supplementary Fig. 1f**). At 14.0 dpc, microglia were only loosely associated with vessels (**Supplementary Fig. 1g**). Microglia engraftment was accompanied by an increase of Iba-1$^+$ CX_3CR1-GFP$^+$ cells in the neuroectoderm (**Supplementary Fig. 2h**) that was mirrored by numerous proliferating cells around 14.0 and 16.0 dpc (**Supplementary Fig. 2i**).

Head macrophages expressed high levels of the maturation factors Mac-1, MCSF-R and F4/80, suggesting a favorable environment for macrophages in the early neuroectoderm (**Supplementary Fig. 3a**). Moreover, the surface molecules CCR2, MCSF-R, F4/80, CD31 and Mac-1 were strongly developmentally regulated (**Supplementary Fig. 3b**). In addition, CD45 was downregulated over time, whereas Mac-1 was highly expressed during development (**Supplementary Fig. 3b,c**). To further define the state of microglia differentiation *in situ*, we performed quantitative single-cell real-time PCR on microdissected yolk sac macrophages, embryonic microglia (dpc 14.0) and adult microglia (postnatal day 60, P60) (**Fig. 2c–e**). We quantified transcripts from genes that are known to be involved in the mesoderm-to-hematopoiesis transition (*Gata2*, *Tal1*), in adult macrophage

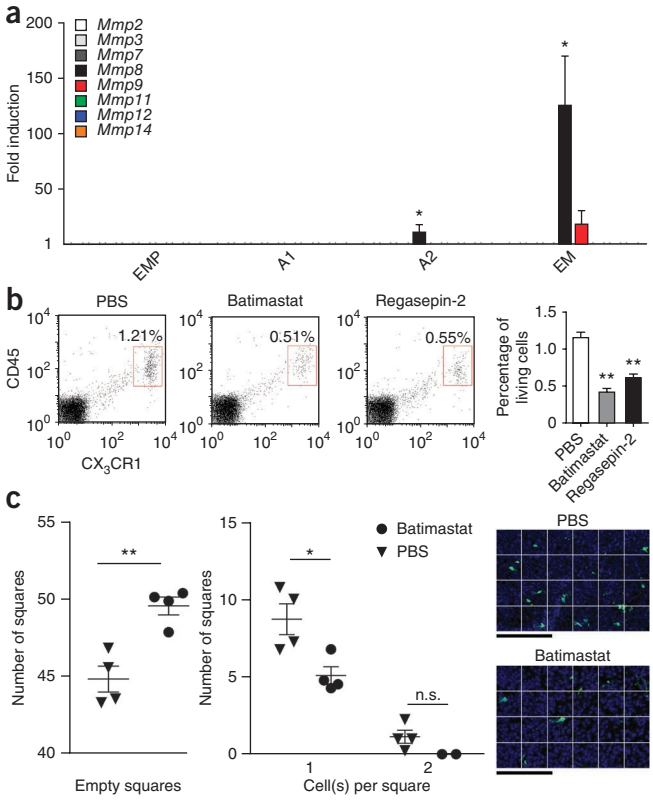

Figure 4 MMPs regulate early microglia expansion. (**a**) Developmental expression of MMPs on isolated cell populations by quantitative RT-PCR normalized to the mean expression value of the particular gene in adult microglia. Bars represent means ± s.e.m. with three mice in each group. $^{*}P < 0.05$. (**b**) Reduced number of CD45^{+} CX$_3$CR1^{+} microglia in the 14.0-dpc neuroectoderm 24 h after Batimastat and Regasepin-2 application in pregnant mice. Representative dot plots (left) and quantification thereof (right). Bars represent means ± s.e.m. with four to six animals in each group. $^{**}P < 0.01$, compared with PBS-treated control mice. (**c**) Left, grid-based cluster analysis of CX$_3$CR1^{+} microglia in the midbrain. One symbol represents the mean value of one individual mouse. Center bars represent the mean of the grouped animals. Error bars represent s.e.m. $^{**}P < 0.01$. n.s., not significant ($P > 0.05$). Right, sections of 14.0-dpc neuroectoderm with CX$_3$CR1^{+} microglia (green), counterstained with DAPI (blue). Scale bar represents 100 µm.

differentiation or myelopoiesis (*Maf*, *Mafb*, *Lyz2*, *Sfpi*), macrophage and microglia activation (*Tlr2*, *Tlr4*, *Mmp2*, *Mmp9*, *Mmp14*), M2 polarization (*Il10*, *Tgfb1*), and dendritic cell differentiation (*Relb*). *Lyz2*, *Sfpi*, *Tlr2*, *Tlr4*, *Mmp2*, *Mmp9*, *Mmp14*, *Gata2* and *Tal1* transcripts were increased in embryonic microglia compared with adult microglia and yolk sac macrophages. In contrast, *Maf* and *Il10* transcripts were detected at significant levels in both embryonic microglia and yolk sac macrophages ($P < 0.05$), whereas adult microglia expressed fewer transcripts of this macrophage differentiation gene. In sum, both yolk sac macrophages and embryonic microglia develop differentially, most likely as a result of the tissue environment that favors macrophage maturation in the neuroectoderm.

MMPs, but not chemokines, modulate microgliogenesis

Given that we had observed that macrophage maturation and migration is associated with the induction of surface molecules, we examined the developmentally regulated expression of chemokine receptors and their ligands in yolk sac precursors (EMPs, A1, A2) and embryonic microglia compared with adult microglia (**Fig. 3**). We found markedly high mRNA levels in distinct progenitor cell populations of the following chemokine and chemokine receptor pairs: *Cxcr3* and *Cxcl4*, *Cx3cr1* and *Cx3cl1*, *Ccr2* and *Ccl2*, and *Ccr1* and *Ccl9* (**Fig. 3a**,**b**). To test the biological relevance of these induced chemoattractant molecules and of the M-CSFR signaling factor Tyrobp (DAP12/KARAP), we evaluated the presence of microglia at 14.0 dpc in the respective knockout strains (**Fig. 3c**). Essentially, we were not able to detect any changes of embryonic microglia numbers and morphology in these mutants. During adulthood, however, Tyrobp deficiency influenced both the numbers and morphology of microglia in several brain regions, indicating a homeostatic rather than a developmental function of this molecule (**Supplementary Fig. 4**). Notably, a reduction of microglia numbers has been reported in mice carrying a natural null mutation in M-CSF, the M-CSFR ligand, without mentioning any morphological changes[16,17]. Our results strongly suggest that the recruitment of the microglia precursors is independent of most of the induced chemokine signals, at least at the single knockout level.

Matrix metalloproteinases (MMPs) form a family of more than 20 enzymes that are involved in the remodeling of extracellular matrix components during acute inflammatory reactions and chronic autoimmune diseases[18]. It is still unclear yet whether MMPs have a functional role during microgliosis. To solve this issue, we first measured the expression levels of several MMPs in embryonic microglia and their progenitor populations (**Fig. 4a**). *Mmp8* and *Mmp9* were found to be highly induced in A2 and embryonic microglia that still needed to crawl in the developing neuroectoderm. To check the biological function of MMPs, we applied several inhibitors and examined the presence of CD45^{+} CX$_3$CR1^{+} embryonic microglia in the 14.0-dpc embryo (**Fig. 4b**). Notably, the broad MMP inhibitor Batimastat significantly reduced the number of CD45^{+} CX$_3$CR1^{+} cells from 1.16 ± 0.06% to 0.42 ± 0.05% in phosphate-buffered saline (PBS)-treated mice ($P < 0.01$). The peptide inhibitor Regasepin-2, which has been shown to inhibit MMP-8 and MMP-9 at the micromolar level *in vitro*[19], was able to decrease the number of CD45^{+} CX$_3$CR1^{+} cells to 0.61 ± 0.048%. We next addressed the question of whether MMP inhibition might impair microglia expansion, and used a grid-based cluster analysis to assess microglia distribution (**Fig. 4c**). Microglia spreading was clearly diminished in Batimastat-treated embryos, suggesting a pivotal role of MMPs for microglia migration.

Microglia development is Pu.1 and Irf8 dependent

In addition to M-CSFR, several transcription factors have been shown to be important for lineage commitment in myeloid cells[20,21]. For example, the balance of Pu.1 protein levels determines the fate of myeloid progenitors, promoting development along either the macrophage or dendritic lineages[22,23]. To determine which transcription factors are required for microglia development, we measured *Myb*, *Runx1*, *Sfpi*, *Irf8*, *Irf4*, *Id2*, *Batf3* and *Klf4* mRNA levels in sorted EMPs, A1 and A2 cells, and embryonic microglia (**Fig. 5a**). All of the transcription factors were only barely detectable in CD45^{-} c-kit^{+} EMPs, whereas significant levels of the myeloid-related transcription factors *Irf8*, *Batf3* and *Klf4* were observed in A1 and A2 cells and embryonic microglia ($P < 0.05$). Notably, *Sfpi* mRNA was continuously expressed during microglia development (EMP, 5.8 ± 1.9–fold induction; A1 cells, 7.4 ± 2.0–fold induction; A2, 3.2 ± 0.3–fold induction; embryonic microglia, 3.0 ± 1.5–fold induction compared with adult microglia).

To assess the effect of these transcription factors on microgliogenesis, we investigated the presence of Iba-1^{+} 14.0-dpc microglia in the

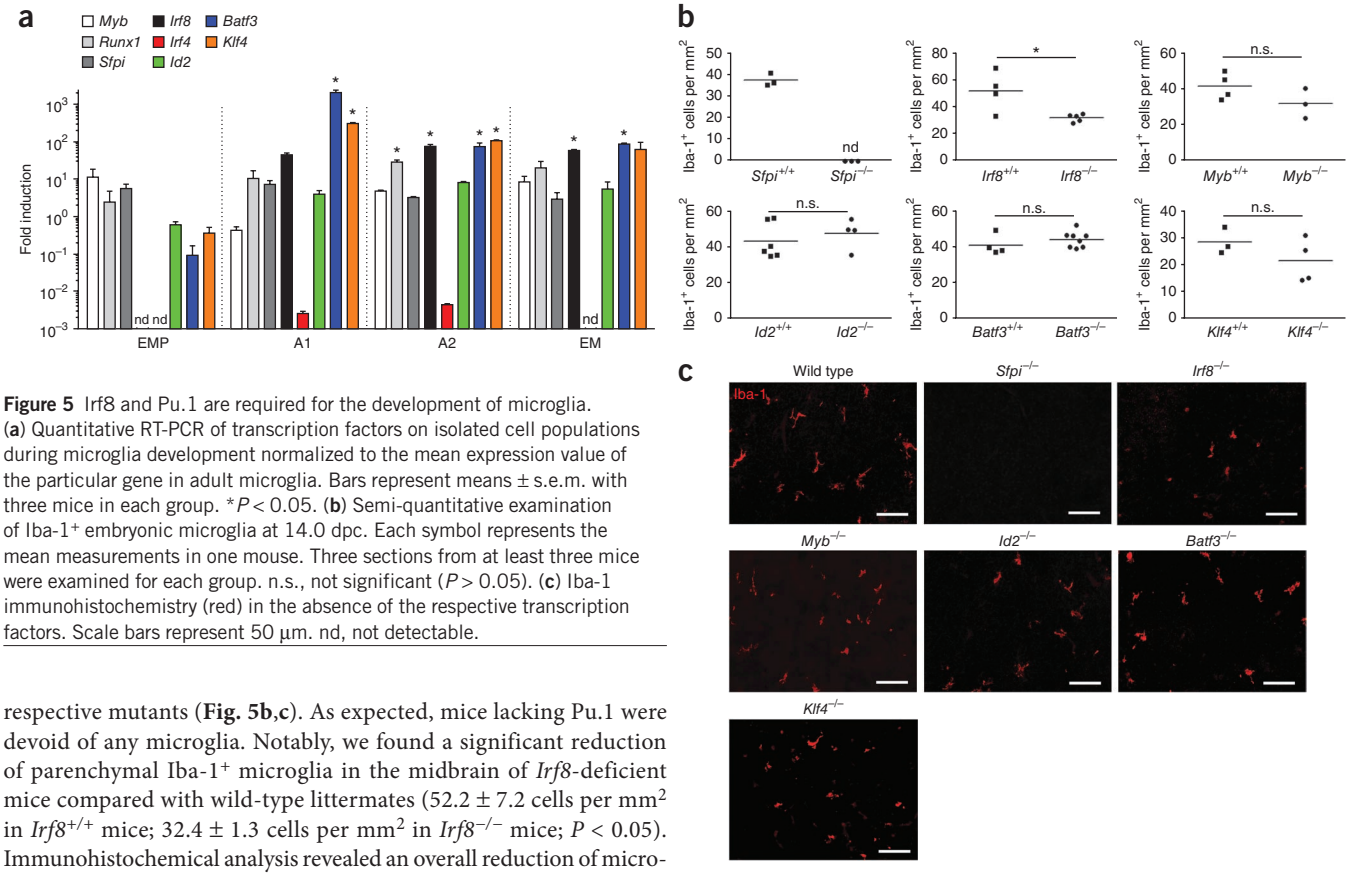

Figure 5 Irf8 and Pu.1 are required for the development of microglia. (**a**) Quantitative RT-PCR of transcription factors on isolated cell populations during microglia development normalized to the mean expression value of the particular gene in adult microglia. Bars represent means ± s.e.m. with three mice in each group. $*P < 0.05$. (**b**) Semi-quantitative examination of Iba-1$^+$ embryonic microglia at 14.0 dpc. Each symbol represents the mean measurements in one mouse. Three sections from at least three mice were examined for each group. n.s., not significant ($P > 0.05$). (**c**) Iba-1 immunohistochemistry (red) in the absence of the respective transcription factors. Scale bars represent 50 μm. nd, not detectable.

respective mutants (**Fig. 5b**,**c**). As expected, mice lacking Pu.1 were devoid of any microglia. Notably, we found a significant reduction of parenchymal Iba-1$^+$ microglia in the midbrain of *Irf8*-deficient mice compared with wild-type littermates (52.2 ± 7.2 cells per mm^2 in *Irf8*$^{+/+}$ mice; 32.4 ± 1.3 cells per mm^2 in *Irf8*$^{-/-}$ mice; $P < 0.05$). Immunohistochemical analysis revealed an overall reduction of microglia density in *Irf8*-deficient animals. Reduced microglia numbers were still present in adult *Irf8*$^{-/-}$ mice and could be confirmed using transmission electron microscopy (**Supplementary Fig. 5a**,**b**). The lack of *Id2*, *Batf3*, *Klf4* and *Myb* did not significantly impair microglia development ($P > 0.05$). Of note, *Myb* deficiency during adulthood did not impair microglia numbers, as was recently shown[8].

To more directly examine the mechanistic cause of microglia decrease in Irf8 and Pu.1 mutants, we analyzed the respective yolk sac progenitor populations (**Fig. 6a**). The c-kit$^+$ population was unaffected by the absence of Irf8 (1.2 ± 0.2% in *Irf8*$^{-/-}$ and 1.0 ± 0.1% in *Irf8*$^{+/+}$). However, *Irf8*-deficient yolk sac specifically had a significantly reduced A2 population (281 ± 73 cells (11.1 ± 2.9% of *Irf8*$^{+/+}$) compared with 2,524 ± 251 cells in *Irf8*$^{+/+}$; $P < 0.001$), but preserved A1 cells, indicating a maturation defect. In contrast, the lack of Pu.1 diminished both the A1 (301 ± 90 cells (12.4 ± 3.7% of *Sfpi*$^{+/+}$) versus 2418 ± 611 cells in *Sfpi*$^{+/+}$) and A2 populations (133 ± 14 cells (9.8 ± 1.0% of *Sfpi*$^{+/+}$) versus 1350 ± 351 cells in *Sfpi*$^{+/+}$), but preserved the c-kit$^+$ population (2.3 ± 0.6% in Sfpi$^{-/-}$ and 0.9 ± 0.3% in *Sfpi*$^{+/+}$). Analysis of the *Irf8*-deficient A1 population revealed that Irf8 is an essential survival factor during early microgliogenesis (**Fig. 6b**). The lack of Irf8 induced significantly more ($P < 0.05$) annexin V$^+$ apoptotic A1 cells (29.9 ± 8.2%) compared with the wild-type situation (5.5 ± 0.9%). However, remaining *Irf8*-deficient A2 cells were still able to differentiate into ramified Iba-1$^+$ microglia in the OHSC system (**Supplementary Fig. 6**).

We next addressed the question whether Pu.1 and Irf8 interact with each other in microglia. We first examined the expression of the transcription factor Runx1 that drives all lineages of hematopoiesis and the myeloid-specific factors Pu.1 and Irf8 (**Supplementary Fig. 7a–c**). All transcription factors were found to be expressed at the RNA level (**Supplementary Fig. 7a**), as proteins (**Supplementary Fig. 7b**) and were clearly localized in the nucleus (**Supplementary Fig. 7c**) in BV2 microglia cells, but not in NIH3T3 fibroblasts. To test whether Irf8 acts downstream of Runx1 and Pu.1, we performed shRNA knockdown experiments using an IRES-GFP construct (**Supplementary Fig. 7d**,**e**). Knockdown of Pu.1 and Runx1 led to reduced nuclear expression of Irf8 in GFP$^+$ transfected cells (shPu.1, 75.6 ± 4.9% of *LacZ* control; shRunx1, 81.8 ± 3.8% of *LacZ* control). Accordingly, PCR and western blot analysis revealed significantly reduced Irf8 levels ($P < 0.05$). Collectively, these data clearly indicate that both Pu.1 and Irf8 function as mutual interaction partners, Irf8 acting downstream of Pu.1.

DISCUSSION

We identified CD45$^-$ c-kit$^+$ erythromyeloid progenitors in the yolk sac as the source of immigrating macrophages in the developing brain and found that these cells represent the direct precursor of the definitive microglia population in the CNS. This developmental process is characterized by a concomitant maturation and differentiation of microglia progenitors via CX_3CR1^- and CX_3CR1^+ stages.

This complex developmental process is obviously independent of major chemokine receptor signaling, but requires MMP-8 and MMP-9. It has been shown that myeloid recruitment to the inflamed CNS is strongly dependent on key chemokines and their receptors, such as CCR2 and its ligand CCL2 (refs. 2,3). Moreover, CCR2 is essential for the extravasation of Ly-6C$^+$ monocytes from the bone marrow[24]. CCR2 expression has been described in early immature macrophages during embryogenesis using *Ccr2*^{RFP} indicator mice[25], with subsequent downregulation of the receptor during development that is consistent with our observation of developmentally regulated *Ccr2* mRNA expression. As microgliogenesis is obviously independent of the investigated chemokine receptors, the process of macrophage

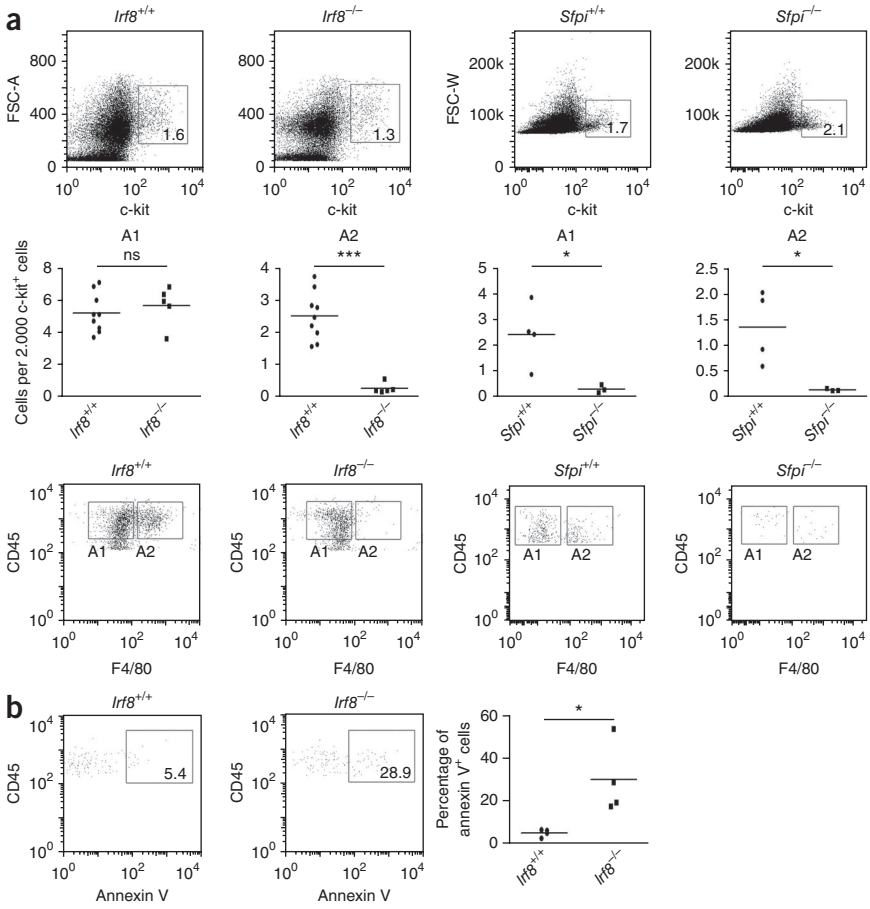

Figure 6 Yolk sac precursors depend on the presence of Irf8 and Pu.1. (**a**) FACS analysis and quantification of A1 and A2 myeloid progenitors in 9.0 dpc embryos lacking Irf8 or Pu.1. Left, quantification thereof. Data represent means ± s.e.m. with at least three mice in each group. Representative dot plots from individual mice are depicted. $*P < 0.05$, $***P < 0.001$. n.s., not significant ($P > 0.05$). (**b**) Percentages of annexin V–expressing apoptotic cells. Each symbol represents one individual mouse. The means are indicated. $*P < 0.05$. Data represent means ± s.e.m. with at least three mice in each group.

and microglia migration during development requires other, as yet unknown, signals. In fact, macrophage engraftment into the neuroepithelium requires an active blood stream[7] that might passively carry the cells.

MMPs form a family of more than 20 enzymes that are involved in the remodeling of extracellular matrix components[18]. They have a functional role in both physiological and pathological conditions. Gelatinase B or MMP-9, which is one of the most structurally complex MMPs, is a known target in acute inflammatory reactions and chronic autoimmune diseases[18]. Our findings that both MMP-9 and MMP-8 are important for the expansion of microglia during embryogenesis indicate new features of MMPs during development (**Supplementary Fig. 8**).

We found that, in the yolk sac, Irf8 and Pu.1 were vital for the proper development of microglia at the A1 and A2 levels, respectively, but not at the stem cell level. Pu.1 is a transcription factor that is expressed exclusively in hematopoietic cells and known to be important for myeloid cell development[20]. *Sfpi*-deficient mice are devoid not only of circulating monocytes and tissue macrophages[26], but also of parenchymal microglia in the brain[8,27]. Similar data have been obtained in Pu.1-deficient zebrafish microglia[28]. Our results indicate that the lack of microglia in *Sfpi*$^{-/-}$ mice is a result of a strong reduction at progenitor cell level, whereas c-kit^{+} EMPs are unaltered in the absence of Pu.1. Our results also suggest an important and unsuspected role for Irf8. Thus, the role of Irf8 in myeloid development appears to be broader than previously reported[29]. How does *Irf8* deficiency induce impaired microglia development? It is well established that both Pu.1 and Irf8 can act simultaneously as heterodimerization partners or, alternatively, they can also function subsequently as downstream targets[30]. We found that Pu.1 deletion in microglia led to a consequent downregulation of Irf8. It is known that Irf8 has broad effects on myeloid cell survival and that it controls the transcriptional response of mature myeloid cells to interferons and Toll-like receptor agonists, a response in which Irf8 binds and transactivates the promoters of *Il12b* and *Nos2*, which encodes inducible nitric oxide synthase[30]. Whereas Pu.1 deficiency resulted in a reduction in the number of A1 and A2 progenitor cells, we found a normal number of A1 progenitor cells and reduced number of A2 cells in *Irf8*-deficient yolk sac, which might be a result of differential expression of both transcription factors during development. Of note, the strong reduction of A2 cells in the absence of Irf8 only led to a mild reduction of microglia numbers compared with the lack of Pu.1, suggesting that both factors can also act independently and that the few remaining A2 cells in *Irf8*$^{-/-}$ mice may later continue to proliferate.

In sum, our data suggest that microglia develop from Irf8- and Pu.1-dependent, Myb-, Id2-, Batf3- and Klf4-independent EMPs. Despite the fact that none of these proteins are specific for microglia, this unique genetic profile distinguishes them from other myeloid cells, such as circulating monocytes, CD11b^{+} dendritic cells and CD8^{+} CD103^{+} CD11b^{-} dendritic cells[21].

METHODS

Methods and any associated references are available in the online version of the paper.

Note: Supplementary information is available in the online version of the paper.

ACKNOWLEDGMENTS

We would like to thank M. Oberle, A. Hölscher and U. Müller for excellent technical assistance, M. Mann for help with the heat map, A. Müller for assistance with the electron microscopy and S. Brendecke for critical reading and editing. The authors are indebted to S. McKercher (Sanford-Burnham Medical Research Institute) for providing *Sfpi*$^{+/-}$ mice and to J. Frampton (University of Birmingham) for providing *Myb*$^{+/-}$ mice. We thank S. Heck and the Flow facility of the Biomedical Research Centre at King's Health Partners. M.P., K.B. and F.R. are supported by the Deutsche Forschungsgemeinschaft (DFG)-funded research unit 1336 "From monocytes to brain macrophages-conditions influencing the fate of myeloid cells in the brain". M.P. is supported by the Bundesministerium für Bildung und Forschung-funded Competence Network of Multiple Sclerosis (Kompetenznetz Multiple Sklerose), the Competence Network of Neurodegenerative Disorders (Deutsches Zentrum für Neurodegenerative Erkrankungen), the Centre of Chronic Immunodeficiency and the DFG (SFB 620, PR 577/8-1). G.F. is supported by a Heisenberg fellowship (DFG FR 1488/3-2). M.H. is supported by the Helmholtz-Zentrum München, a European Research Council starting grant and the Swiss National Foundation. G.O. is supported by

the Geconcentreerde OnderzoeksActies 2012/017 and the Fund for Scientific Research-Flanders. C.S. is supported by a fellowship program of the German National Academy of Sciences Leopoldina (LPDS 2009-31). F.G. is supported by grants MRCG0900867 from the Medical Research Council and ERC-2010-StG-261299 from the European Research Council.

AUTHOR CONTRIBUTION

M.P. designed the project, analyzed the data and wrote the manuscript. K.K., F.R., M.H., G.F. and F.G. designed parts of the project and analyzed the results. K.K., D.E., C.S., E.G.P., P.W., A.H., P.R., T.G., V.S. and K.B. performed the experiments. C.H., D.N.M., B.L., T.B., K.D., G.O. and A.D. provided genetically modified animals and inhibitors and analyzed the results.

COMPETING FINANCIAL INTERESTS

The authors declare no competing financial interests.

Published online at http://www.nature.com/doifinder/10.1038/nn.3318.
Reprints and permissions information is available online at http://www.nature.com/reprints/index.html.

1. Hanisch, U.K. & Kettenmann, H. Microglia: active sensor and versatile effector cells in the normal and pathologic brain. *Nat. Neurosci.* **10**, 1387–1394 (2007).
2. Ransohoff, R.M. & Perry, V.H. Microglial physiology: unique stimuli, specialized responses. *Annu. Rev. Immunol.* **27**, 119–145 (2009).
3. Prinz, M., Priller, J., Sisodia, S.S. & Ransohoff, R.M. Heterogeneity of CNS myeloid cells and their roles in neurodegeneration. *Nat. Neurosci.* **14**, 1227–1235 (2011).
4. Prinz, M. & Mildner, A. Microglia in the CNS: immigrants from another world. *Glia* **59**, 177–187 (2011).
5. Chan, W.Y., Kohsaka, S. & Rezaie, P. The origin and cell lineage of microglia: new concepts. *Brain Res. Rev.* **53**, 344–354 (2007).
6. Alliot, F., Godin, I. & Pessac, B. Microglia derive from progenitors, originating from the yolk sac, and which proliferate in the brain. *Brain Res. Dev. Brain Res.* **117**, 145–152 (1999).
7. Ginhoux, F. *et al.* Fate mapping analysis reveals that adult microglia derive from primitive macrophages. *Science* **330**, 841–845 (2010).
8. Schulz, C. *et al.* A lineage of myeloid cells independent of Myb and hematopoietic stem cells. *Science* **336**, 86–90 (2012).
9. Geissmann, F., Jung, S. & Littman, D.R. Blood monocytes consist of two principal subsets with distinct migratory properties. *Immunity* **19**, 71–82 (2003).
10. Jung, S. *et al.* Analysis of fractalkine receptor CX(3)CR1 function by targeted deletion and green fluorescent protein reporter gene insertion. *Mol. Cell. Biol.* **20**, 4106–4114 (2000).
11. Takahashi, K., Naito, M. & Takeya, M. Development and heterogeneity of macrophages and their related cells through their differentiation pathways. *Pathol. Int.* **46**, 473–485 (1996).
12. Palis, J., Robertson, S., Kennedy, M., Wall, C. & Keller, G. Development of erythroid and myeloid progenitors in the yolk sac and embryo proper of the mouse. *Development* **126**, 5073–5084 (1999).
13. Palis, J. *et al.* Spatial and temporal emergence of high proliferative potential hematopoietic precursors during murine embryogenesis. *Proc. Natl. Acad. Sci. USA* **98**, 4528–4533 (2001).
14. Bertrand, J.Y. *et al.* Three pathways to mature macrophages in the early mouse yolk sac. *Blood* **106**, 3004–3011 (2005).
15. Vinet, J. *et al.* Neuroprotective function for ramified microglia in hippocampal excitotoxicity. *J. Neuroinflammation* **9**, 27 (2012).
16. Wegiel, J. *et al.* Reduced number and altered morphology of microglial cells in colony stimulating factor-1–deficient osteopetrotic op/op mice. *Brain Res.* **804**, 135–139 (1998).
17. Otero, K. *et al.* Macrophage colony-stimulating factor induces the proliferation and survival of macrophages via a pathway involving DAP12 and beta-catenin. *Nat. Immunol.* **10**, 734–743 (2009).
18. Hu, J., Van den Steen, P.E., Sang, Q.X. & Opdenakker, G. Matrix metalloproteinase inhibitors as therapy for inflammatory and vascular diseases. *Nat. Rev. Drug Discov.* **6**, 480–498 (2007).
19. Hu, J. *et al.* Inhibition of lethal endotoxin shock with an L-pyridylalanine containing metalloproteinase inhibitor selected by high-throughput screening of a new peptide library. *Comb. Chem. High Throughput Screen.* **9**, 599–611 (2006).
20. Rosenbauer, F. & Tenen, D.G. Transcription factors in myeloid development: balancing differentiation with transformation. *Nat. Rev. Immunol.* **7**, 105–117 (2007).
21. Geissmann, F. *et al.* Development of monocytes, macrophages, and dendritic cells. *Science* **327**, 656–661 (2010).
22. Bakri, Y. *et al.* Balance of MafB and PU.1 specifies alternative macrophage or dendritic cell fate. *Blood* **105**, 2707–2716 (2005).
23. Anderson, K.L. *et al.* Transcription factor PU.1 is necessary for development of thymic and myeloid progenitor–derived dendritic cells. *J. Immunol.* **164**, 1855–1861 (2000).
24. Serbina, N.V. & Pamer, E.G. Monocyte emigration from bone marrow during bacterial infection requires signals mediated by chemokine receptor CCR2. *Nat. Immunol.* **7**, 311–317 (2006).
25. Mizutani, M. *et al.* The fractalkine receptor, but not CCR2, is present on microglia from embryonic development throughout adulthood. *J. Immunol.* **188**, 29–36 (2012).
26. McKercher, S.R. *et al.* Targeted disruption of the PU.1 gene results in multiple hematopoietic abnormalities. *EMBO J.* **15**, 5647–5658 (1996).
27. Beers, D.R. *et al.* Wild-type microglia extend survival in PU.1 knockout mice with familial amyotrophic lateral sclerosis. *Proc. Natl. Acad. Sci. USA* **103**, 16021–16026 (2006).
28. Herbomel, P., Thisse, B. & Thisse, C. Zebrafish early macrophages colonize cephalic mesenchyme and developing brain, retina and epidermis through a M-CSF receptor–dependent invasive process. *Dev. Biol.* **238**, 274–288 (2001).
29. Hambleton, S. *et al.* IRF8 mutations and human dendritic-cell immunodeficiency. *N. Engl. J. Med.* **365**, 127–138 (2011).
30. Taniguchi, T., Ogasawara, K., Takaoka, A. & Tanaka, N. IRF family of transcription factors as regulators of host defense. *Annu. Rev. Immunol.* **19**, 623–655 (2001).

ONLINE METHODS

Mice. *Cx3cr1*$^{GFP/wt}$ mice were a kind gift of D. Littman (New York University School of Medicine). *Dap12*$^{-/-}$ mice were obtained from T. Takai (Tohoku University). *Ccr2*$^{-/-}$ and actin-Ds-tomato (B6.129(Cg)-Gt(ROSA)26Sor$^{tm4(ACTB-tdTomato,-EGFP)Luo}$/J) mice were purchased from Jackson Laboratory. *Ccr1*$^{-/-}$ mice were kindly provided from B. Luckow (Kliniken der Universität München), *Cxcr3*$^{-/-}$ and *Tyrobp*$^{-/-}$ mice from C. Hölscher (Research Center Borstel), *Irf8*$^{-/-}$ mice from F. Rosenbauer (University of Muenster), *Id2*$^{-/-}$ mice from Y. Yokota (University of Fukui), *Batf3*$^{-/-}$ mice from K. Murphy (Washington University), and *Klf4*$^{-/-}$ mice from K. Kaestner (University of Pennsylvania). Mice were bred in-house under pathogen-free conditions. Both male and female mice were used in this study. The animal experiments were performed in accordance with the guidelines of Bezirksregierung Freiburg legislation for animal experiments. The animal permission numbers are G-11/46, X-12/06H, X-11/10H and X-10/08H.

Quantification of microglia/macrophage engraftment in the CNS. Time pregnancy was performed to obtain the embryos at defined time points after conceptions. Pregnant females with vaginal plugs were determined as 0.5 dpc. Whole embryos were embedded and processed. For adult brain sections, mice were transcardially perfused with PBS followed by 4% paraformaldehyde (wt/vol), and 20-µm cryosections were obtained. Primary and preabsorbed antibodies were added overnight at a dilution of 1:500 for Iba-1 (019-19741, WACO), 1:500 for F4/80 (MCA497R, Serotec), 1:1,000 for nestin (MAB353, Chemicon International), 1:500 for CD45 (550539, BD Pharmingen), 1:250 for LAMP-2 (ab13524, Abcam) and 1:100 for Rhodamine-labeled Isolectin B4 (RL-1102, Vector Laboratories) at 4 °C. Alexa Fluor 555–conjugated secondary antibodies (A21428, A31570 and A21434, Invitrogen) were added at a dilution of 1:500 for 2 h at 20–25 °C. Nuclei were counterstained with 4,6-diamidino-2-phenylindole (DAPI). GFP-expressing ramified cells and Iba-1$^+$ or F4/80$^+$ macrophages/microglia were counted in at least three sections from each individual mouse. The number of cells was examined microscopically using a 200-fold microscopical magnification using a conventional fluorescence microscope (Olympus BX-61) equipped with a color camera (Olympus DP71).

Isolation of hematopoietic cells from yolk sac and FACS analysis. Yolk sacs were dissected from staged embryos and dissected from the embryo proper. Single-cell suspensions were prepared by mechanical homogenization in FACS buffer (1% fetal calf serum in PBS). Cell suspensions were stained for CD45 (30-F11), c-kit (2B8), CD11b (M1/70), MCSF-R (AFS98), F4/80 (BM8) or annexin V (eBioscience, BD Pharmingen). Cell suspensions were acquired on a FACS Canto II (Becton Dickinson) or cell populations were sorted with a MoFlo Astrios (Beckman Coulter) and further processed. Data were analyzed with FlowJo.

Microglia isolation and FACS analysis. Murine microglia from adult mice, 14.0 dpc and 16.0 dpc were harvested using density gradient separation as described recently[31]. For flow cytometry analyses CNS samples were prepared as described previously[31]. In short, samples were stained for CD11b, CD45, MCSF-R, F4/80, CD31 (390), Ki67 (20Raj1) (eBioscience, BD Pharmingen) or CCR2 (MC-21 antibody as described recently[32]). Cell suspensions were acquired on a FACS Canto II (Becton Dickinson) or cell populations were sorted with a MoFlo Astrios (Beckman Coulter) and further processed. Data were analyzed with FlowJo.

Gene expression analysis. Sorted cell populations were collected in cell lysis buffer and RNA was isolated with an Arcturus Pico Pure RNA Isolation Kit (Life Technologies) according to the manufacturer's instructions. Reverse transcription, preamplification and gene expression analysis were done with SA Biosciences PCR array reagents (Qiagen). RT-PCR arrays were analyzed with a LightCycler 480 (Roche) and peqSTAR 96 (peqlab). For gene expression analysis, we used the following primers: Pu.1 forward (5′-cctgcgtctgacccacgacc-3′), Pu.1 reverse (5′-tcatccgatggaggggcggtg-3′), Runx1 forward (5′-acaggctttcgcagagcggtga-3′), Runx1 reverse (5′-agcgcctcgctcatcttgcc-3′), IRF8 forward (5′-gcgaagttcctgag atggag-3′) and IRF8 reverse (5′-tctgggagaaagctgaatgg-3′).

OHSCs and methylcellulose assays. OHSCs and microglia depletion were performed as described previously[15]. In brief, slice cultures were prepared from 2–3-d-old mouse pups under sterile conditions. After decapitation, the brains were removed and the hippocampi from both hemispheres were acutely isolated in ice-cold serum-free Hank's Balanced Salt Solution, supplemented with 0.5% glucose (wt/vol, Sigma Aldrich) and 15 mM HEPES. Isolated hippocampi were cut into 350–375-µm-thick slices using a tissue chopper (McIlwain) and were transferred to 0.4-µm culture plate inserts (Millipore, PICM03050). These culture plate inserts, containing four to six slices, were placed in six-well plates containing 1.2 ml of culture medium per well. Culture medium (pH 7.2) consisted of 0.5× minimum essential medium (MEM) containing 25% heat-inactivated horse serum, 25% BME basal medium without glutamate, 2 mM glutamax and 0.65% glucose. The slice cultures were kept at 35 °C in a humidified atmosphere (5% CO_2) and the culture medium was refreshed the first day after preparation and every 2 d thereafter. Endogenous microglia were depleted by incubation with approximately 0.5 mg ml^{-1} Lip-CL solution (1:10 liposome dilution in standard slice culture medium) for 24 h at 35 °C. Subsequently, the slice cultures were carefully rinsed in PBS (35 °C) to wash away residual liposomes and placed on fresh culture medium. After depletion, the medium was refreshed every 2 d. Both vehicle-treated slice cultures and slice cultures treated with empty liposomes served as controls. For the adoptive transfer of yolk sac cells, 400 cells of each yolk sac population were isolated: CD45$^+$ CX_3CR1^- and CD45$^+$ CX_3CR1^+ cells from 10.5-dpc *Cx3cr1*$^{GFP/+}$ embryos and CD45$^+$ c-kit$^-$, CD45$^-$ c-kit$^-$ and CD45$^-$ c-kit$^+$ from 8.0-dpc *Cx3cr1*$^{GFP/+}$ embryos, followed by direct transfer onto OHSCs. OHSCs were shortly rinsed in PBS (35 °C) 12 d after transfer and fixed with 4% paraformaldehyde overnight at 4 °C. After fixation, the slice cultures were rinsed in PBS and pre-incubated with 5% normal goat serum (NGS, Vector) in PBS containing 0.3% Triton X-100 (PBS$^+$) for at least 1 h. Subsequently, the slice cultures were incubated with the appropriate primary antibodies overnight in 1% NGS/PBS$^+$ at 4 °C. Primary and preabsorbed antibodies were added overnight at a dilution of 1:500 for Iba-1 (WACO) or 1:500 for F4/80 (Serotec). To support myeloid colony formation, sorted yolk sac progenitors were brought to methylcellulose cultures and cultured as described previously[33]. After 7 d and 28 d, colonies were analyzed by flow cytometry for their differentiation and cytospins were prepared from individual colonies. To evaluate myeloid differentiation, cytospins were stained with Pappenheim.

Slice preparation of adult CNS and morphological analysis. We obtained 30-µm cryo sections from adult brain tissue. Free floating sections were stained overnight at a dilution of 1:500 for Iba-1 (WACO), followed by Alexa Fluor 555–conjugated secondary antibody staining (Invitrogen), which was added at a dilution of 1:500 for 2 h at 20–25 °C. Nuclei were counterstained with DAPI. Imaging was performed on an Olympus Fluoview 1000 confocal laser-scanning microscope (Olympus) using a 20× 0.95 NA objective. *z* stacks were done with 1.1-µm steps in *z* direction, 1,024 × 1,024 pixel resolution were recorded and analyzed using IMARIS software (Bitplane).

***In vivo* MMP inhibitor treatment.** At 13.0 dpc, pregnant females were injected intraperitoneally with 600 µg Batimastat (Merck), intravenously with 700 µg Regasepin2 or with a vehicle control. Pregnant mice were killed 24 h after injection and embryos were dissected. Embryonic microglia were isolated and used for FACS analysis or embryos were fixed in 4% paraformaldehyde and further processed for immunochemistry.

Laser microdissection and electron microscopy. Microdissection of 100 yolk sac macrophages, embryonic and adult microglia respectively was performed using a Zeiss PALM MicroBeam (Zeiss) as described previously with modifications[32,34]. Fast immunochemistry of serial sections from embryonic and adult tissue was performed with F4/80 antibody (Serotec). Immunostained sections were counterstained with DAPI to facilitate the identification of individual cells. RNA was isolated with the RNeasy Micro Plus Kit (Qiagen) and reverse transcription, preamplification and real-time PCR were performed using Applied Biosystems reagents as described previously[35] and according to the manufacturer's recommendations. For electron microscopy sections from epon-embedded, glutaraldehyde-fixed cortices were cut and stained with toluidine blue. The tissue was then trimmed and reoriented so that ultrathin cross sections of the cortices could be cut and treated with uranyl acetate and lead citrate. Electron micrographs were analyzed for the numbers of microglia cells per area.

Knockdown analysis. shRNA hairpin sequences of Pu.1 and Runx1 were cloned into psi-RNA h7SK-GFPzeo vector (Invivogen). NIH3T3 fibroblasts and BV-2 cells were grown in DMEM GlutaMAX (Invitrogen) supplemented with 10% fetal calf serum (PAA) and 1% penicillin/streptomycin (PAA) at 37 °C and 5% CO_2. Transfections were performed using X-tremeGENE HP (Roche), according to the manufacturer's protocol. Medium was changed 24 h after transfection. For western blot analysis, cells were harvested and extracted in RIPA buffer (25 mM Tris-HCl, 150 mM NaCl, 1% Nonidet P-40, 0.5% sodium deoxycholate, 0.1% SDS, pH 7.5). Samples were separated by SDS-PAGE and immunoblotted using antibodies to Pu.1 (1:1,000, sc-352, Santa Cruz Biotech), Runx1 (1:1,000, ab23980, Abcam), Irf8 (1:1,000, sc-6058, Santa Cruz Biotech) and actin (1:2,000, sc-1616, Santa Cruz Biotech). Band intensities were obtained using ImageJ software. For immunofluorescence analysis, transfected cells were fixed with 4% paraformaldehyde, incubated with 0.01% Tween-20 in PBS, blocked in 5% BSA and incubated with primary antibodies for Irf8 (1:100, sc-6058, Santa Cruz Biotech) in blocking reagent overnight. Subsequently, cells were washed and Alexa Fluor 555–conjugated secondary antibodies (Invitrogen) were added at a dilution of 1:500 for 2 h at 20–25 °C. Nuclei were counterstained with DAPI.

Statistical analysis. Statistical differences were evaluated using a non-paired Student's *t* test. Differences were considered to be significant when $P < 0.05$.

31. Mildner, A. *et al.* Microglia in the adult brain arise from Ly-6C(hi)CCR2(+) monocytes only under defined host conditions. *Nat. Neurosci.* **10**, 1544–1553 (2007).
32. Mildner, A. *et al.* Distinct and nonredundant roles of microglia and myeloid subsets in mouse models of Alzheimer's disease. *J. Neurosci.* **31**, 11159–11171 (2011).
33. Akashi, K., Traver, D., Miyamoto, T. & Weissman, I.L. A clonogenic common myeloid progenitor that gives rise to all myeloid lineages. *Nature* **404**, 193–197 (2000).
34. Raasch, J. *et al.* I{kappa}B kinase 2 determines oligodendrocyte loss by non-cell-autonomous activation of NF-{kappa}B in the central nervous system. *Brain* **134**, 1184–1198 (2011).
35. Dann, A. *et al.* Cytosolic RIG-I–like helicases act as negative regulators of sterile inflammation in the CNS. *Nat. Neurosci.* **15**, 98–106 (2012).

doi:10.1038/nn.3318

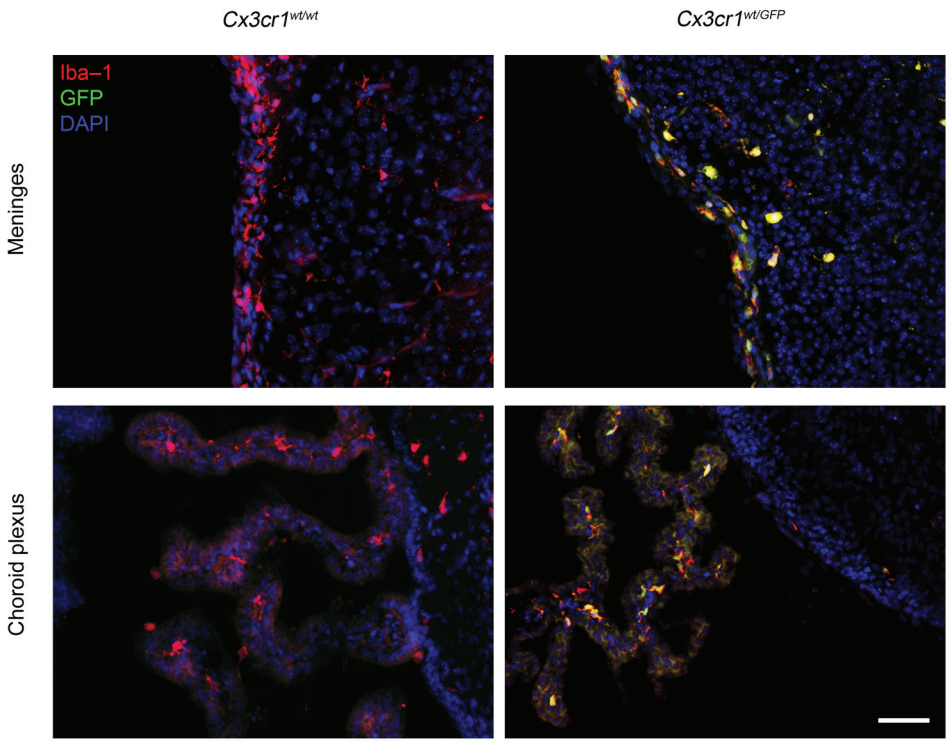

Suppl. Figure 1

Nature Neuroscience: doi:10.1038/nn.3318

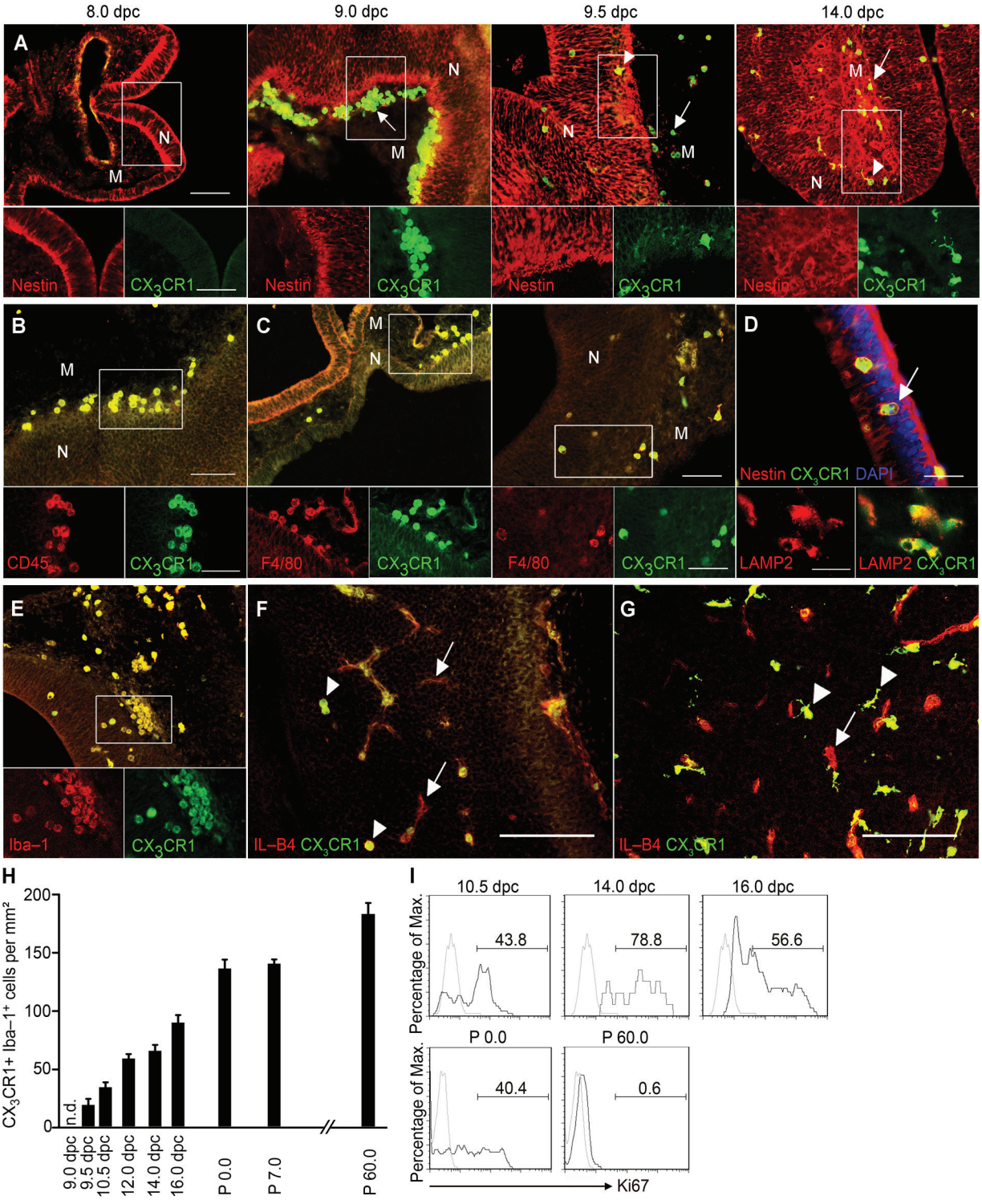

Suppl. Figure 2

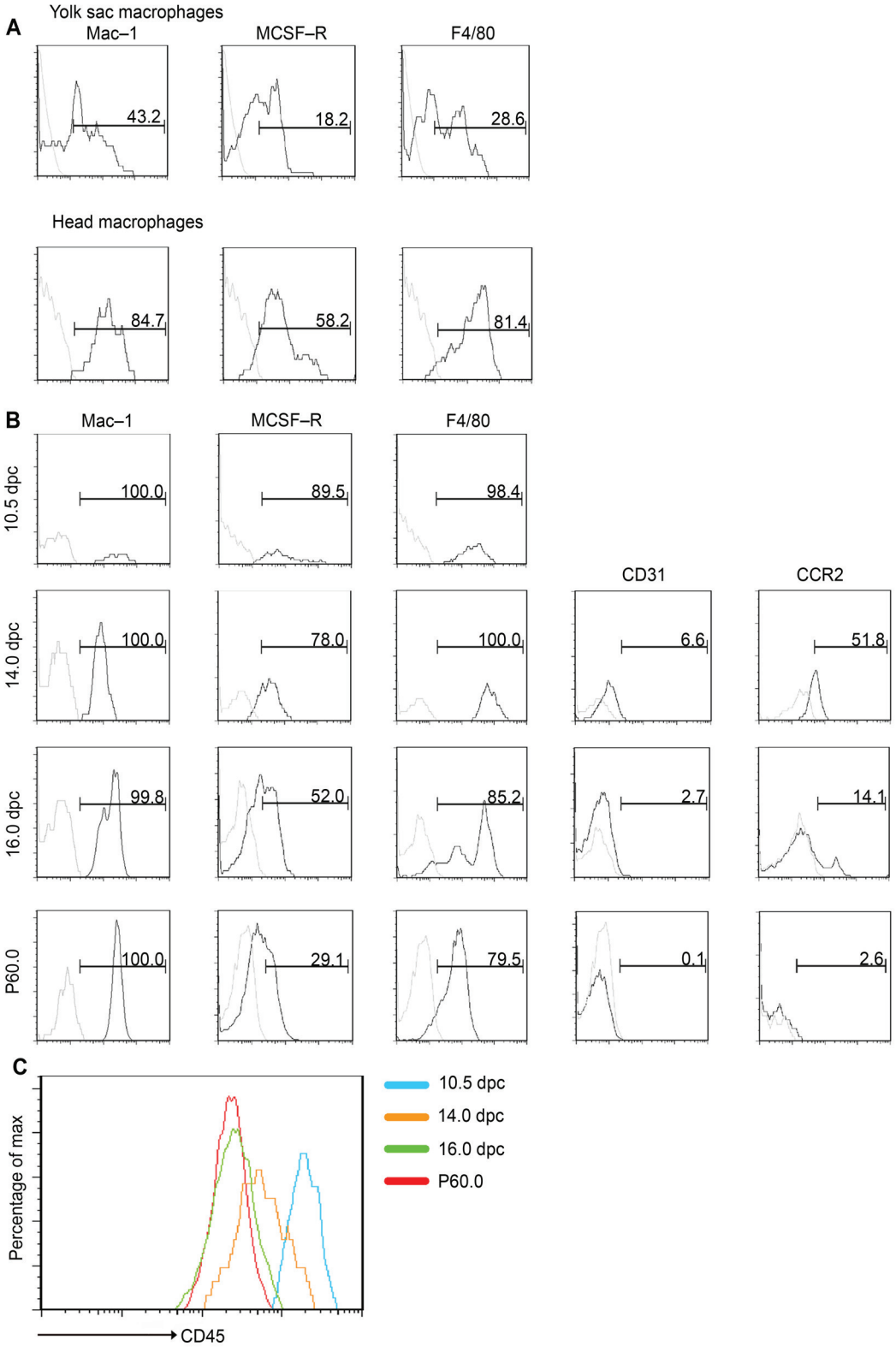

Suppl. Figure 3

Nature Neuroscience: doi:10.1038/nn.3318

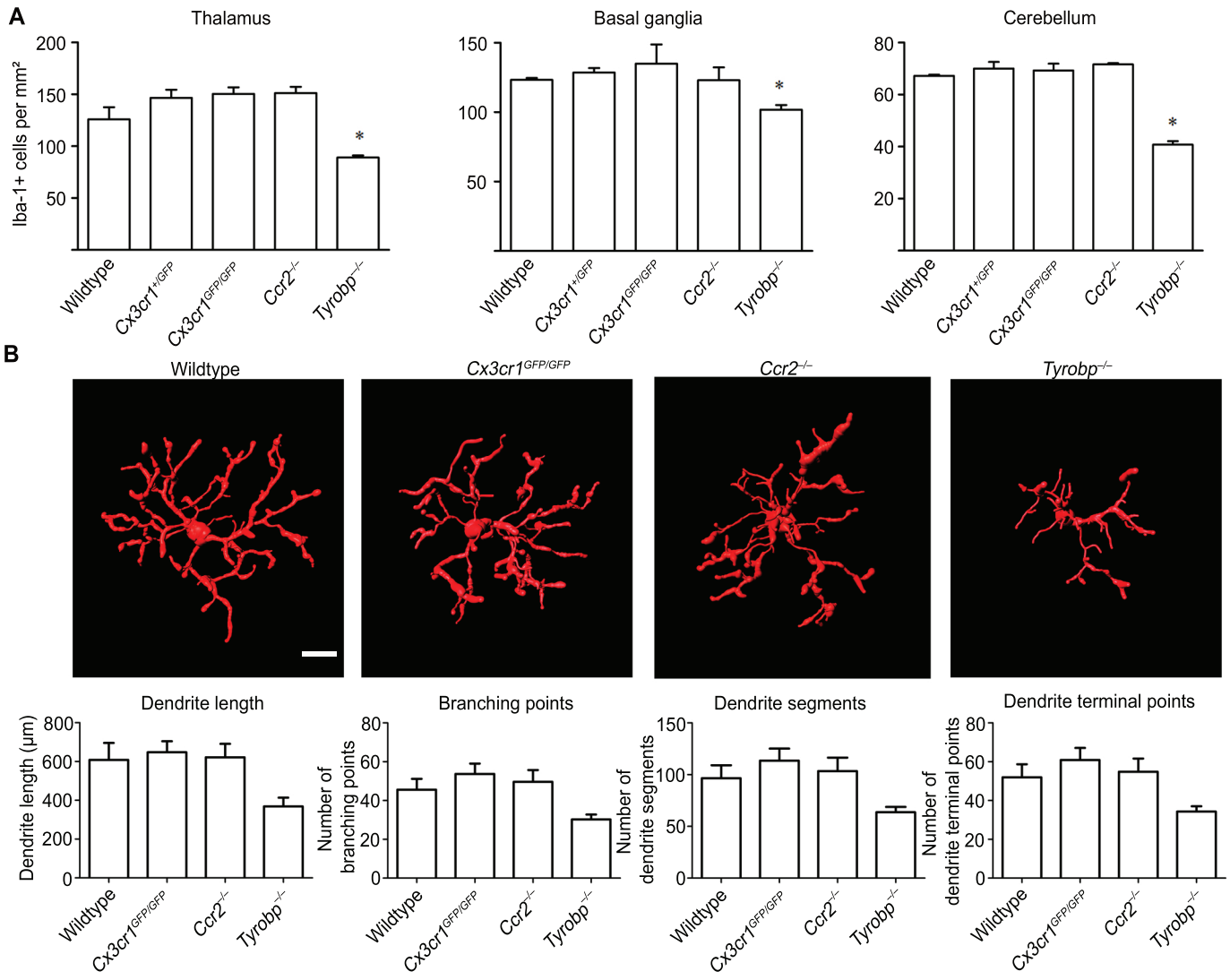

Suppl. Figure 4

Nature Neuroscience: doi:10.1038/nn.3318

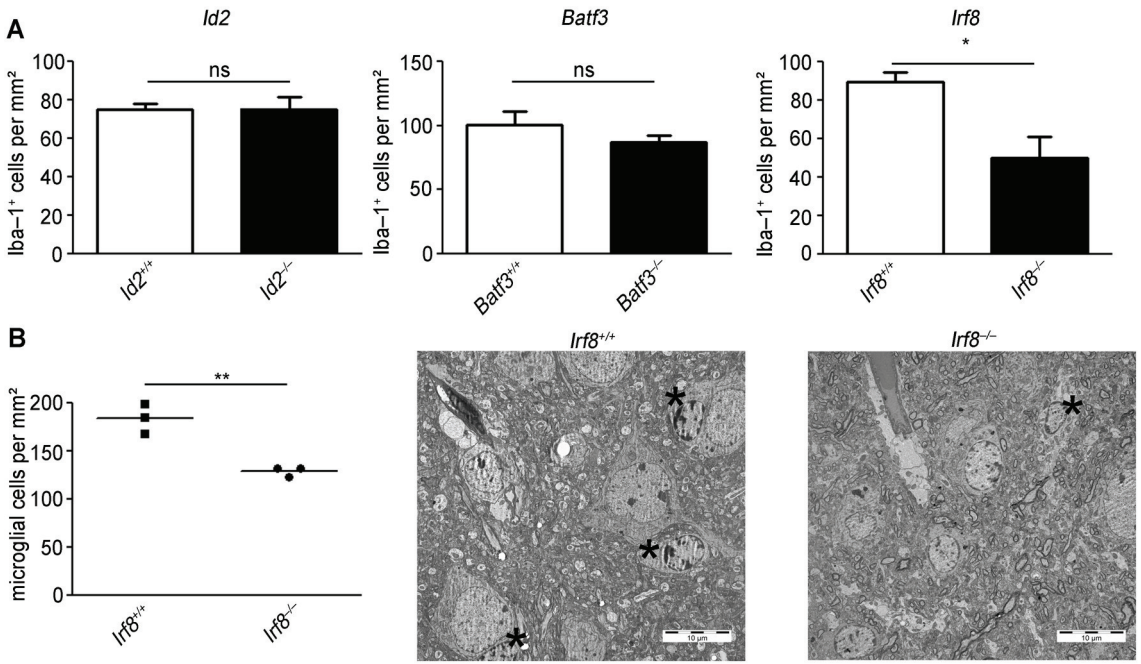

Suppl. Figure 5

Nature Neuroscience: doi:10.1038/nn.3318

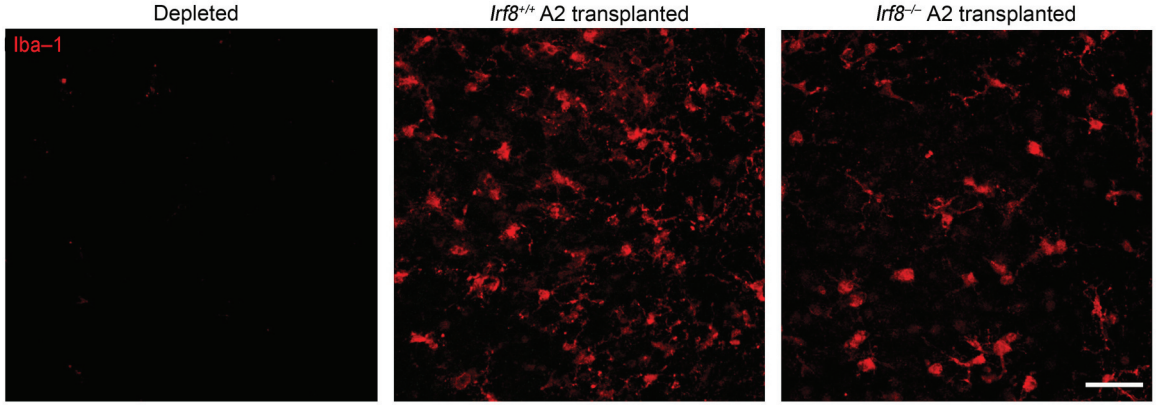

Suppl. Figure 6

Nature Neuroscience: doi:10.1038/nn.3318

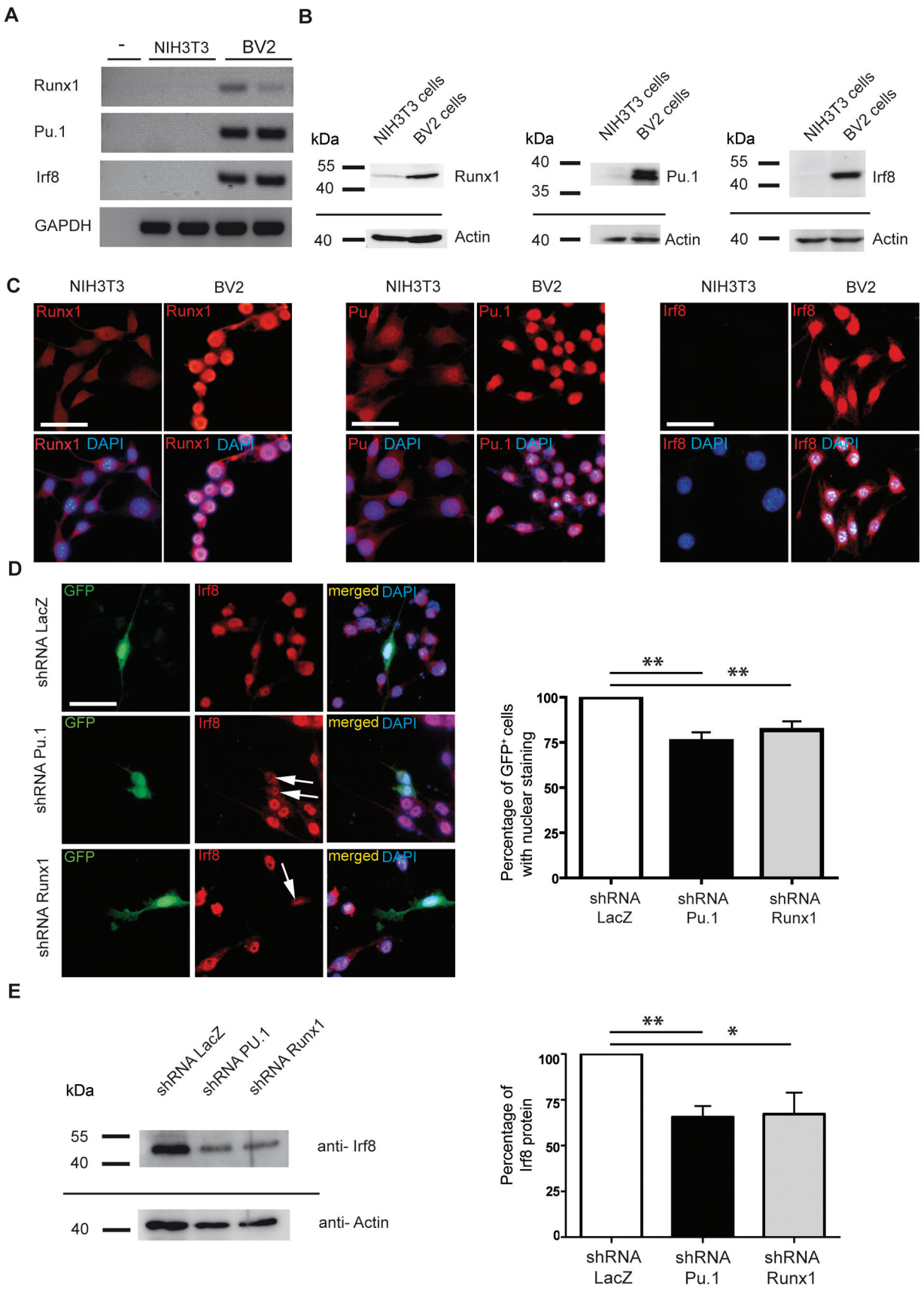

Suppl. Figure 7

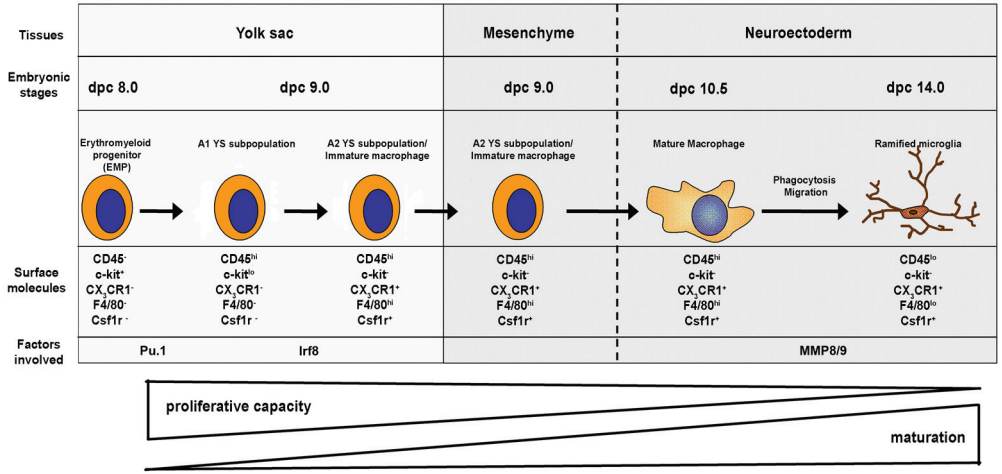

Suppl. Figure 8

Nature Neuroscience: doi:10.1038/nn.3318

SUPPLEMENTARY FIGURES

Supplementary Figure 1: No maternally-derived microglia in the embryo meninges and choroid plexus.

Left panel: Direct fluorescent microscopic visualization revealed no maternal GFP^+ cells in meninges and choroid plexus of newborns. Iba-1 immunoreactivity (red) for microglia/macrophages and DAPI staining for nuclei (blue) in $CX_3CR1^{wt/wt}$ embryos. Scale bars:100 µm. Right panel: Visualization of $CX_3CR1\text{-}GFP^+$ $Iba\text{-}1^+$ meningeal and choroid plexus macrophages in *Cx3cr*$^{GFP/wt}$ littermates. Scale bars: 100 µm.

Supplementary Figure 2: Macrophage maturation and development into definitive microglia in the embryonic brain.

(A) Sagittal brain sections at different stages of embryogenesis from 8.0 to 14.0 dpc depicting the neural tube (N, nestin, red), *Cx3cr1*$^{GFP/+}$ myeloid cells (green) and the adjacent mesenchyme (M). As early as 9.0 dpc round *Cx3cr1*$^{GFP/+}$ macrophages first appear in the mesenchyme adjacent to the neuroectodermal border. *Cx3cr1*$^{GFP/+}$ macrophages start seeding the neuroectoderm at 9.5 dpc but show typical microglia morphology such as round to spindle-shaped soma and a distinct arborization pattern as early as 14.0 dpc. Arrows mark macrophages and arrowheads indicate microglia. Scale bars: 100 µm (overviews) and 50 µm (inserts). Immunofluorescence for CD45 **(B)** (red) and the macrophage maturation marker F4/80 at 9.0 dpc **(C**, red, left) and F4/80 at 9.5 dpc **(C**, red. left). Scale bar: 100 µm (overviews) and 50 µm (inserts). **(D)** Direct fluorescent microscopic visualization reveals highly phagocytotic *Cx3cr1*$^{GFP/+}$ ameboid microglia (green, arrow) with ingested nuclei as visualized by $DAPI^+$ fluorescence (blue) in the neural tube (N, nestin, red) at 12.0 dpc (upper panel). Scale bar: 50 µm. Strong lysosomal LAMP activity (red) at 12.0 dpc (lower panel). Scale bar: 20 µm. **(E)** Immunofluorescence for the macrophage marker Iba-1 (red). **(F)** Isolectin-B_4 (IL-B_4) fluorescence staining for freshly seeded amoeboid microglia (arrowheads) and vessels (arrows) in the neural tube at the onset of vascularization at 9.5 dpc and **(G)** during vessel outgrowth at 14.0 dpc. **(H)** Semi-quantitative analysis of regional $CX_3CR1^+Iba\text{-}1^+$ macrophage/microglia numbers in the CNS at different time points of development. Data are expressed as means ± s.e.m. of three sections of three to five animals per group. **(I)** Proliferation capacity of microglia precursors and fully differentiated microglia analyzed by FACS for Ki-67. Only $CD45^+$ GFP^+ cells were gated and the percentages of Ki-67 expressing cells are depicted. Data are representative of two independent experiments.

Nature Neuroscience: doi:10.1038/nn.3318

Supplementary Figure 3: Macrophage maturation and development into definitive microglia in the embryonic brain.

(A) Flow cytometry of myeloid precursors in the YS and head at 10.5 dpc for M-CSFR, F4/80 and MAC-1. **(B)** Maturation of $CD45^+GFP^+$ microglia from *Cx3cr1*$^{GFP/+}$ mice from 10.5 dpc to postnatal day 60 (P60) by using the markers CCR2, M-CSFR, F4/80, CD31 and MAC-1 for FACS. Data are representative of two to three independent experiments. Representative cytometry graphs of the three independent experiments are depicted. Grey lines indicate the isotype controls, black lines the antibody staining. Percentages of positively labeled cells compared to isotype controls are shown. **(C)** Surface CD45 expression on developing microglia. Representative graphs of $CD11b^+GFP^+$ cells from pooled $CX_3CR1^{GFP/+}$ brains are shown. Data are representative of two independent experiments.

Supplementary Figure 4: Tyrobp (DAP12) but not CX_3CR1 or CCR2 deficiency influences microglia numbers and morphology in the adult brain.

(A) Quantification of Iba-1^+ parenchymal microglia in adult (P60) brains devoid of CX_3CR1, CCR2 or Tyrobp. Three sections of at least three mice were examined for each group. Bars represent means ± s.e.m. Asterisks indicate statistical significance (* = *p<0.05*). **(B)** 3-D structure and automatic analysis of microglia morphology. Bars represent means ± S.E.M. three cells of three animals per group.

Supplementary Figure 5: Irf8 but not Id2 or Batf3 deficiency shapes microglia number in the adult brain.

(A) Quantitative examination of Iba-1^+ parenchymal cortical microglia in adult (P60) brains lacking the transcription factors Id2, Batf3 or Irf8. Three sections of at least three mice were examined for each group. Bars represent means ± s.e.m.. Asterisks indicate statistical significance (* = *p<0.05*). **(B)** Electron microscopical evaluation of neocortical microglia in Irf-8-deficient mice or negative littermates. Left: Quantification of microglia numbers. Each symbol represents the mean measurements in one animal. Three grids of at least three mice were examined for each group. Asterisks indicate statistical significance (** = *p<0.01*). Right: Transmission electron microscopy in cortices of *Irf-8*$^{-/-}$ and *Irf-8*$^{+/+}$ animals. Asterisks point to individual microglia cells.

Supplementary Figure 6: Differentiation of *Irf8*-deficient A2 cells into microglia.

A2 cells YS cells were adoptively transferred on organotypic hippocampal brain slice cultures depleted of endogenous microglia. At day 12 in culture transferred cells were analyzed using the macrophage marker Iba-1. Scale bar = 50 µm.

Nature Neuroscience: doi:10.1038/nn.3318

Supplementary Figure 7: Irf-8 acts in microglia downstream of the transcription factors Pu.1 and Runx1.

(A) PCR expression analysis for *Runx1*, *Sfpi* and *Irf8* transcripts in NIH3T3 fibroblasts and BV2 microglia cells. *Gapdh* was used as control. One representative experiment out of three is shown. **(B)** Western blot analysis of cellular lysates for Runx1, Pu.1 and Irf8. Actin served as loading control. One experiment out of two is depicted. **(C)** Direct fluorescent microscopic visualization reveals expression of Runx1, Pu.1 and Irf8 (red) in the nuclei ($DAPI^+$ fluorescence [blue]) of cultured cells. Scale bars: 10 µm. **(D)** Left: Immunofluorescence for nuclear expression of Irf8 (red) in the nuclei ($DAPI^+$ fluorescence [blue]) 48 h after transfection with shRNA constructs. Arrows point to GFP^+ cells with diminished Irf8 expression. Right: Quantification thereof. Scale bars: 10 µm. One experiment out of three similar ones is shown. **(E)** Immunoblot for Irf8 48 h after transfection with shRNA plasmids (left) and quantification (right).

Supplementary Figure 8: Schema of microglia development

Summary of the proposed differentiation steps of microglia progenitors on the basis of our current findings. Defined stages of microgliogenesis occur in distinct parts of the YS and developing brain, respectively.

Nature Neuroscience: doi:10.1038/nn.3318

making. This mismatch is intimately connected with the genesis of teenage angst. Puberty and its associated angst is a period of heightened vulnerability to emotional or social insult[15], and poorly controlled decision making during this time can have a lifetime of consequences. The more we understand about puberty and how it is controlled, the better for all of us.

COMPETING FINANCIAL INTERESTS
The author declares no competing financial interests.

1. Herbison, A.E. *Horm. Res.* **68** (suppl. 5), 75–79 (2007).
2. Wade, G.N., Schneider, J.E. & Li, H.Y. *Am. J. Physiol.* **270**, E1–E19 (1996).
3. Lomniczi, A. *et al. Nat Neurosci* **16**, 281–289 (2013).
4. Grumbach, M.M. *Horm. Res.* **57** (suppl. 2), 2–14 (2002).
5. Kasuya, E., Nyberg, C.L., Mogi, K. & Terasawa, E. *Endocrinology* **140**, 705–712 (1999).
6. Seminara, S.B. & Crowley, W.F. Jr. *J. Neuroendocrinol.* **20**, 727–731 (2008).
7. Ebling, F.J. & Luckman, S.M. *Endocrinology* **149**, 899–901 (2008).
8. Kauffman, A.S. *Mol. Cell Endocrinol.* **324**, 51–63 (2010).
9. Prezioso, C. & Orlando, V. *FEBS Lett.* **585**, 2067–2077 (2011).
10. Bernstein, B.E. *et al. Cell* **125**, 315–326 (2006).
11. Wagner, I.V. *et al. Nat. Rev. Endocrinol.* **8**, 246–254 (2012).
12. Elias, C.F. *Trends Endocrinol. Metab.* **23**, 9–15 (2012).
13. Fowler, P.A. *et al. Mol. Cell Endocrinol.* **355**, 231–239 (2012).
14. Bianco, S.D. *Front. Endocrinol.* (*Lausanne*) **3**, 149 (2012).
15. Sisk, C.L. & Foster, D.L. The neural basis of puberty and adolescence. *Nat. Neurosci.* **7**, 1040–1047 (2004).

Brain microglia: watchdogs with pedigree

Harald Neumann & Hartmut Wekerle

Microglia have been regarded as the tissue macrophages of the brain. A study now finds that microglia are quite distinct from blood-borne macrophages and derive from an erythromyeloid precursor cell of the embryonic hematopoiesis.

The tissues of the CNS are generally considered to be immunologically privileged, evading full control by immune surveillance. But they are by no means left defenseless: they are protected by cellular watchdogs, the microglia. The brain parenchyma is sown with these microglial cells, which are very special myeloid phagocytes that occupy and govern individual tissue territories, responding immediately and vigorously to the appearance of any undesirable materials[1] (degenerated or apoptotic cells, tumor cells, and infectious organisms) and igniting classic innate immune responses. Moreover, once activated, microglia can link to the more specific adaptive immune response, productively presenting antigens to reactive lymphocytes. As such, microglia cells resemble resident macrophages and dendritic cells in peripheral tissues, functioning in the brain as immunological watchdogs that raise the alarm against intruders and, if necessary, assault them. It now seems that these microglial watchdogs descend from a highly distinct pedigree. A study by Kierdorf *et al.*[2] in this issue of *Nature Neuroscience* shows that microglia stem from primitive erythromyeloid progenitors. These are cells competent to give rise to either red blood cells or early macrophage lineages. They reach the CNS early in embryonic development and, at their CNS destination, gradually assume definitive microglial properties.

Harald Neumann is at the Institute of Reconstructive Neurobiology, University Bonn, Bonn, Germany, and Hartmut Wekerle is at the Max Planck Institute of Neurobiology, Martinsried, Germany.
e-mail: hwekerle@neuro.mpg.de

As was already known, microglia are of mesodermal origin, which sets them apart from the neuroectodermal neurons, astrocytes and oligodendrocytes. Their morphology and phagocytic function is strongly reminiscent of tissue resident and perivascular macrophages, but their origin differs radically. Whereas the latter derive from classic hematopoietic stem cells that persist throughout life in stem cell niches (the bone marrow, in the adult) and reach their target tissues via the bloodstream[3], the precursors of microglia invade the brain from the yolk sac. As was discovered recently, this happens at a very early stage of embryonic development[4]; however, the cellular ancestors giving rise to the microglia had not been pinpointed.

Studying a sophisticated set of transgenic mice, Kierdorf *et al.*[2] identified the microglial progenitors from the yolk sac as erythromyeloid precursor cells. Passing through an intermediate stage (marker profile: $CD45^+$ c-kit^{lo} CX_3CR1^- F4/80^- $CD115^-$) at embryonic day 9.0 (E9.0), the early descendants assume the characteristics of immature macrophages ($CD45^+$ c-kit^- CX_3CR1^+ F4/80^+ $CD115^+$) and become mobile. They leave their yolk sac habitat at E9.0, ultimately at E10.5 invading the structures destined to give rise to the brain[2]. Thus, microglia derive from early committed macrophages, which were previously described as descendants of a second wave of primitive hematopoiesis in the yolk sac[5]. The steps that drive erythromyeloid precursors to intermediate proliferating cells and to immature macrophages are controlled by the myeloid transcriptional factors Pu.1 and IRF8, respectively. However, early microglial development does not require the factors Myb, Id2, Batf3 and Klf4, which is in contrast with that of other myeloid cell populations, clearly distinguishing the microglial developmental program from the differentiation of other myeloid cell types, such as circulating monocytes and dendritic cells[6].

Thus, microglia derive from the transient early embryonic hematopoiesis (EHp). To place this finding in context, EHp is a 'primitive' process restricted to a limited episode of early embryonic development; it is later replaced by the 'definitive', life-long hematopoiesis (DHp) (**Fig. 1**). The two blood-forming pathways build on founder cells with different developmental potential. EHp derives from the aforementioned bipotent erythromyeloid precursors, which selectively give rise to red blood cell and macrophage lineages, and does not depend on the transcriptional activator Myb. In contrast, DHp's founders, multipotent stem cells able to replenish a complete hematopoietic system, do depend on Myb[7].

The finding that microglia are derived from EHp and not from DHp is noteworthy in itself. It is even more surprising that these progenitors migrate into the neuroectodermal brain primordium, settle there permanently and function autonomously throughout adulthood, disconnected from the bone marrow progenitor niches under normal conditions[2,8].

Is this local self-renewing autonomy unique to microglia? According to conventional wisdom, tissue-resident macrophages are derived from recirculating progenitors, mostly blood monocytes, and these are continuously replaced by incoming young monocytes supplied by the bone marrow, the site of ongoing DHp. The absolute validity of this concept has been challenged by very recent observations, which assign at least some limited self-renewal capacity to some macrophage populations in

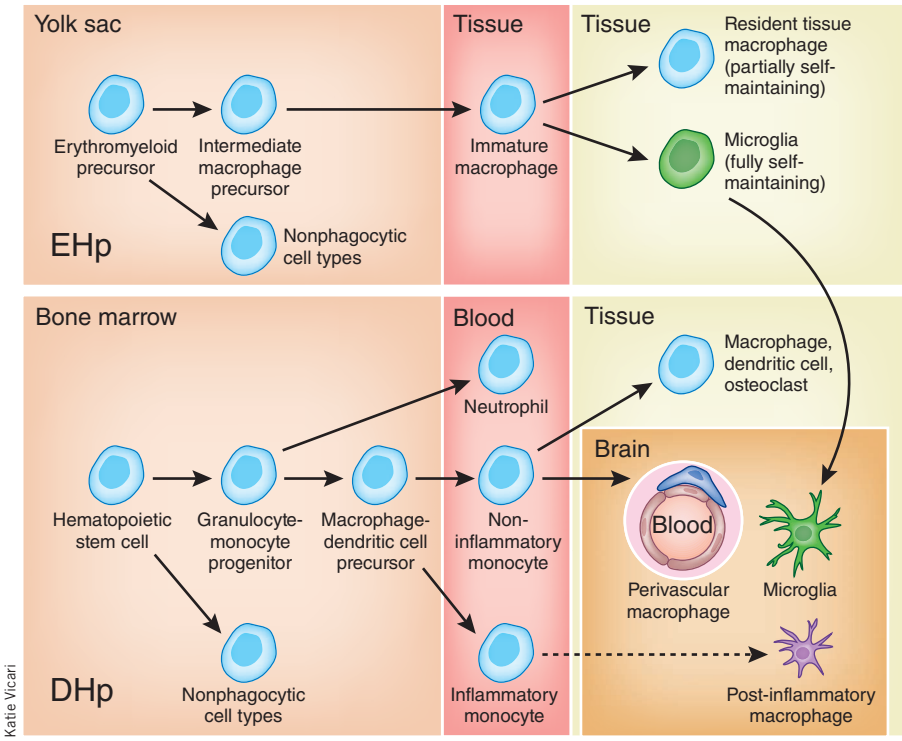

Figure 1 Pedigrees of microglial and macrophage lineages. Microglia (green) are derived from immature phagocytes of the embryonic hematopoiesis (EHp), which migrate from the yolk sac through the primitive vascular system into the neuroepithelium. Their progenitor is an erythromyeloid precursor cell that only exists in the embryo and whose developmental potency is limited to macrophages and erythrocyte lineages. In contrast, the multipotent hematopoietic stem cell of the definitive hematopoiesis (DHp) is located in the adult bone marrow. Most tissue resident macrophages, including the perivascular brain macrophages (dark blue), which are confined by the blood-brain barrier to a space around the blood vessels, are derived from DHp. Brain microglia are a fully self-maintaining population and are not replenished from the blood under normal conditions. However, under exceptional conditions, such as autoimmune diseases or massive loss of microglia, inflammatory CCR2$^+$ monocytes derived from the DHp are admitted into the brain and become post-inflammatory macrophages (purple) with microglia-like features.

peripheral organs such as the liver, skin and spleen[9], albeit not in the perivascular space of the brain, with its perivascular and leptomeningeal phagocytes, the direct neighbors of microglia[10]. The development of these locally self-renewing macrophage populations is, like that of microglia, Myb independent[7]. However, in contrast with the microglia, these extra-neural macrophage populations tend to be slowly replaced in the adult mouse by macrophages derived from the DHp[2,7–9].

Why are these and the other recent findings important? They both change a time-honored concept of brain immunity and will help us to better understand pathological brain conditions. We now recognize that, under normal, homeostatic conditions, microglia form a stable, self-contained population, a closed society, that occupies the brain from very early embryonic development. The individual microglial cells occupy and control individual territories and are replaced by locally proliferating successors, rather than by incoming monocytes. This self-renewing autonomy ceases, however, under pathological conditions. Peripheral phagocytes enter the CNS from the blood and stay there following inflammatory responses, such as in experimental autoimmune encephalomyelitis, a mouse model of multiple sclerosis. Apparently, a massive loss of microglia initiates an emergency program that allows the replenishment of the brain by inflammatory CCR2$^+$ monocytes[11]. This happens, for example, in CD11b-HSVTK transgenic mice, a model designed to allow large-scale ablation of microglia at will, where ablation yields repopulation by new Iba-1$^+$ myeloid cells within a few weeks. The infiltrators are CCR2$^+$ monocytes derived from DHp in the bone marrow[11]. Although the overall distribution of the newly arrived cells resembles that of native microglia, their morphological appearance remains different from that of the resident microglia up to 27 weeks after invasion[11]. Thus, the CNS milieu does not seem to assimilate the incoming phagocytes readily and completely, and the degree to which the functions of local microglia can be assumed by immigrant CCR2$^+$ monocytes remains to be determined.

Why is the CNS colonized so early by microglia and why are their lineages sequestered throughout a lifetime? The explanation could be in their function: microglial cells are credited with an elaborate set of functions beyond tissue protection. Their surface membranes are decorated with an abundance of receptors, including, in addition to sensors of innate immunity, receptors for neurotransmitters and for a variety of trophic factors. This specialized set of signaling structures enables microglial cells to interact with neurons as intimate partners[12]. With their neurotransmitter receptors, microglia cells receive neuronal signals, and they answer by releasing mediators that affect neuronal activity and survival. Conversely, neuronal activity emits signals that modulate microglial inflammatory potential. Of particular importance, microglia are capable of removing synaptic connections, a process that was termed synaptic stripping[13], and of harnessing components of complement, the innate immune effector system[14]. This contributes to neuronal plasticity, in both the developing and adult brain. Finally, there is evidence that microglial cells affect mobilization and induction of neurogenic progenitor cells in their niches[15], another way in which they help keep the tissue of the brain intact.

Such a repertoire of sophisticated functions should require a particularly differentiated, specialized cell, rather than a 'simple' macrophage. Thus, development of the microglial phenotype may be the result of life-long co-evolution with the elements of the brain milieu, a specialization that could not easily be achieved by freshly immigrant monocyte precursors.

The delineation of a separate pedigree of microglia by Kierdorf *et al.*[2] will fuel a variety of investigations. For example, such work should elucidate the nature of the signals inducing the microglial phenotype. Would it be possible to instruct blood-borne macrophages to fully replace degenerating microglia? In a more practical vein, it should intensify the search for specific markers of microglia distinguishing these from circulating macrophages, a search that so far has remained futile.

COMPETING FINANCIAL INTERESTS
The authors declare no competing financial interests.

1. Nimmerjahn, A., Kirchhoff, F. & Helmchen, F. *Science* **308**, 1314–1318 (2005).
2. Kierdorf, K. *et al. Nat. Neurosci.* **16**, 273–280 (2013).
3. Hickey, W.F. & Kimura, H. *Science* **239**, 290–292 (1988).
4. Ginhoux, F. *et al. Science* **330**, 841–845 (2010).

5. Bertrand, J.Y. *et al. Blood* **106**, 3004–3011 (2005).
6. Geissmann, F. *et al. Science* **327**, 656–661 (2010).
7. Schulz, C. *et al. Science* **336**, 86–90 (2012).
8. Massberg, S. *et al. Cell* **131**, 994–1008 (2007).
9. Yona, S. *et al. Immunity* **38**, 79–91 (2012).
10. Ransohoff, R.M. & Cardona, A.E. *Nature* **468**, 253–262 (2010).
11. Varvel, N.H. *et al. Proc. Natl. Acad. Sci. USA* **109**, 18150–18155 (2012).
12. Kettenmann, H., Kirchhoff, F. & Verkhratsky, A. *Neuron* **77**, 10–18 (2013).
13. Blinzinger, K. & Kreutzberg, G.W. *Z. Zellforsch.* **85**, 145–157 (1968).
14. Schafer, D.P. *et al. Neuron* **74**, 691–705 (2012).
15. Sierra, A. *et al. Cell Stem Cell* **7**, 483–495 (2010).

Circuits supporting the grid

Matthew Lovett-Barron & Attila Losonczy

Two studies show that local inhibitory connectivity and hippocampal excitatory input support the spatial firing patterns of entorhinal grid cells, providing support for continuous attractor model of grid cell firing.

When searching for the neural circuit basis of behavior, researchers have historically focused on sensory systems in which neural activity can be reliably evoked with external stimuli. Inconveniently, cognition relies on internally generated activity in the nervous system, a poorly understood process that limits its experimental accessibility for the study of neural circuits. A notable exception is the spatial representation system in the hippocampus and parahippocampal cortices, where the action potential output of neurons conveys information about an animal's location in physical space. In the medial entorhinal cortex (MEC), so-called grid cells fire action potentials when an animal passes through regularly spaced locations that tile their entire environment in a hexagonal pattern[1]. This pattern of spiking provides the animal with a two-dimensional cognitive map of space and provides experimenters with a uniquely reliable neural signature of internally generated activity. This pattern of neural activity has inspired many modeling efforts to gain insight into the underlying circuit mechanisms[2]. Despite the predictions from modeling studies, however, most experimental studies of grid cells to date have been descriptive, with little data available for discerning the underlying circuit mechanisms and to constrain models. In this issue of *Nature Neuroscience*, two companion studies provide crucial experimental support for a specific model of grid cell generation in the MEC of the rat. Taken together, these findings describe how the firing patterns of grid cells arise from local circuitry[3] and extrinsic input[4], providing evidence for a continuous attractor network based on recurrent inhibition and driven by external excitation from the hippocampus.

To determine how MEC grid cells communicate with one another, Couey *et al.*[3] investigated the synaptic connectivity among stellate cells in layer II, a population of excitatory neurons that frequently display grid firing. They assessed synaptic connectivity by targeting multiple layer II neurons for simultaneous patch-clamp recordings in rat brain slices. By triggering action potentials in one or more neurons and recording the postsynaptic potentials in others, the authors were able to reliably assess the presence and strength of synaptic connections between cells. The authors recorded from over 600 pairs of stellate cells and found that there was little or no recurrent excitation among stellate cells. This wiring rule is distinct from that in other neocortical areas, where dense recurrent excitation between principal neurons is the norm. Even so, Couey *et al.*[3] found that stellate cells have an indirect synaptic influence on each other through polysynaptic GABAergic inhibition. Spiking stellate cells excited local GABAergic interneurons, which in turn inhibited neighboring stellate cells. Inhibition was triggered more effectively in stellate cells when multiple neighboring stellate cells were simultaneously spiking in high-frequency bursts, indicating that the probability of inhibition increased as a function of active stellate cells. Surprisingly, this inhibitory input was not graded, but instead appeared as an all-or-none synaptic event of constant amplitude. This even persisted when higher numbers of inputs were synchronously driven by optical activation of many channelrhodopsin-2–expressing stellate cells. This stands in contrast with superficial layers of sensory cortex, where recurrent excitation is present and recurrent inhibition increases in amplitude with the number of excited principal cells[5]. The authors also used multiple intracellular recordings to identify the type of interneurons that couple stellate cells together; fast-spiking local interneurons inhibited roughly half of the recorded stellate cells, whereas connections from low threshold–spiking cells were sparse. This indicates that, at least in layer II, stellate cells and fast-spiking cells act in a closed circuit to promote this inhibitory surround.

It has been reported that grid cells in the MEC stabilize around the third or fourth week of postnatal life[6,7]. If recurrent inhibitory circuitry in the MEC is the cellular foundation that underlies grid firing, then the developmental timescale of recurrent inhibition should match. Indeed, Couey *et al.*[3] found that mice younger than 2 weeks of age lack recurrent inhibition, and even have some recurrent excitation. Between 3 and 4 weeks of age, recurrent excitation drops to zero and inhibitory connectivity reaches adult levels, supporting the authors' conclusions about the importance of recurrent inhibition for grid cell firing.

Given that stellate cells mutually inhibit each other and lack reciprocal excitation, what is the source of the excitatory drive that causes stellate cells to spike in a grid pattern during navigation? A potential source is the hippocampal place cell population, which is itself a target of layer II grid cells. Hippocampal place cells fire action potentials at one specific location in space and send a powerful projection back to the entorhinal cortex, terminating in deep and superficial MEC[8]. To determine the influence of hippocampal excitation on MEC grid cells, Bonnevie *et al.*[4] identified grid cells by means of extracellular electrodes that recorded action potentials from individual MEC neurons in rats that walked around a 100–150-cm box. The authors measured spiking patterns while infusing the $GABA_A$ receptor agonist muscimol into the dorsal hippocampus to inactivate it (**Fig. 1**). They found that bilateral inactivation of the hippocampus disrupted the grid cell map, causing firing fields to become diffuse and irregular. Disruption of grid cell firing was strongly associated with a reduction

Matthew Lovett-Barron and Attila Losonczy are in the Department of Neuroscience, Columbia University, New York, New York, USA. Attila Losonczy is also at the Kavli Institute for Brain Science, Columbia University, New York, New York, USA.
e-mail: al2856@columbia.edu